

1 **Reconstructing past hydrology of eastern Canadian boreal catchments using elastic**
2 **varved sediments and hydro-climatic modelling: 160 years of fluvial inflows**

3
4
5 Antoine Gagnon-Poiré¹⁻⁵, Pierre Brigode², Pierre Francus¹⁻³⁻⁵, David Fortin¹⁻⁶, Patrick
6 Lajeunesse⁴⁻⁵, Hugues Dorion⁴ and Annie-Pier Trottier⁴⁻⁵

7
8 ¹ *Institut national de la recherche scientifique, Centre Eau Terre Environnement*

9 ² *Université Côte d'Azur, CNRS, OCA, IRD, Géoazur, Nice, France.*

10 ³ *Canada Research Chair in Environmental sedimentology and GEOTOP, Research*
11 *Centre on the Dynamics of the Earth System, Montréal, QC, Canada.*

12 ⁴ *Département de géographie, Université Laval, Québec, QC, Canada.*

13 ⁵ *Centre d'études nordiques, Québec, QC, Canada.*

14 ⁶ *Department of Geography and Planning, University of Saskatchewan, Saskatoon, SK,*
15 *Canada*

16
17 Corresponding author: Antoine Gagnon-Poiré (Antoine.Gagnon-Poire@ete.inrs.ca)

18 **Abstract**

19 Analysis of short sediment cores collected in Grand Lake, Labrador, revealed that this lake
20 is an excellent candidate for the preservation of laminated sediments record. The great
21 depth of Grand Lake, the availability of fine sediments along its tributaries, and its
22 important seasonal river inflow have favoured the formation of a 160 years-long clastic
23 varved sequence. Each varve represents one hydrological year. Varve formation is mainly
24 related to spring discharge conditions with minor contributions from summer and autumn
25 rainfall events. The statistically significant relation between varve parameters and the
26 Naskaupi River discharge observations provided the opportunity to develop local
27 hydrological reconstructions beyond the instrumental period. The combined detrital layer
28 thickness and the particle size (99th percentile) series extracted from each varve yield the
29 strongest correlations with instrumental data ($r = 0.68$ and 0.75) and have been used to
30 reconstruct Naskaupi River mean and maximum annual discharges, respectively, over the
31 1856-2016 period. The reconstructed Q-mean series suggest that high Q-mean years
32 occurred during the 1920-1960 period and a slight decrease in Q-mean takes place during
33 the second half of the 20th century. Independent reconstructions based on rainfall-runoff
34 modelling of the watershed from historical reanalysis of global geopotential height fields
35 display a significant correlation with the reconstructed Naskaupi River discharge based on
36 varve physical parameters. The Grand Lake varved sequence contains a regional
37 hydroclimatic signal, as suggested by the statistically significant relation between the
38 combined detrital layer thickness series and the observed Labrador region Q-mean series
39 extracted from five watersheds of different sizes.

40

41 **1. Introduction**

42 Climate changes caused by rising concentrations of greenhouse gases can alter hydro-
43 climatic conditions on inter- and intra-regional scales (Linderholm et al., 2018; Ljungqvist
44 et al., 2016; Stocker et al., 2013). Hydropower, which is considered as a key renewable
45 energy source to mitigate global warming, has strong sensitivity to changes in hydrological
46 regime especially in vulnerable northern regions (Cherry et al., 2017). Therefore, a clear
47 understanding of the regional impacts that recent climate change combined with natural
48 climate variability can have on river discharge and hydroelectric production is needed.

49 However, the lack of instrumental records and the uncertainty related to hydroclimate
50 variability projections (Collins et al., 2013) are obstacles to sustainable management of
51 these water resources.

52

53 The Labrador region in eastern Canada is a critical area for hydropower generation, hosting
54 the Churchill River hydroelectric project, one of the largest hydropower systems in the
55 world. Average annual streamflow has been varying in eastern Canada during the last fifty
56 years, with higher river discharges from 1970 to 1979 and 1990 to 2007, and lower
57 discharges from 1980 to 1989 (Mortsch et al., 2015; Déry et al., 2009; Jandhyala et al.,
58 2009; Sveinsson et al., 2008; Zhang et al. 2001). These changes in streamflow represent a
59 significant economic challenge for the long-term management of hydropower generation.
60 The few decades of available instrumental observations (<60 years) and their low spatial
61 coverage are not sufficient to allow a robust analysis of multi-decadal hydrological
62 variability.

63

64 The study of multi-decadal hydrological variability requires long instrumental records
65 (>100 years), but such long-time series are non-existent for the Labrador region. Recently,
66 rainfall-runoff modelling approaches have been used to expand instrumental streamflow
67 datasets, using long-term climatic reanalysis as inputs. Rainfall-runoff modelling was used
68 by Brigode et al. (2016) to reconstruct daily streamflow series over the 1881–2011 period
69 in northern Québec. Nevertheless, this type of method suffers from the limited observations
70 in order to evaluate and validate the reconstructed hydro-climatic temporal series. The
71 deficiency of observations led to the exploration of various natural archives for
72 reconstructing past hydro-climatic conditions. Long hydro-climatic series based on natural
73 proxies in eastern Canada are rare, limited to a tree ring (Boucher et al., 2017; Begin et al.,
74 2015; Naulier et al., 2015; Nicault et al., 2014; Boucher et al., 2011; Begin et al., 2007;
75 D'Arrigo et al., 2003) and pollen datasets (Viau et al., 2009) and mainly focused on
76 temperature reconstructions. Reconstructing river hydrological series using dendrological
77 analysis is complex in the boreal region due to the indirect relation between tree-ring
78 indicators and streamflow. One study has reconstructed streamflow variations over the last
79 two centuries in Labrador based on tree-ring isotopes series (Dinis et al., 2019). Still, the

80 spatial coverage of palaeohydrological records from independent proxies must be increased
81 in this region. In this perspective, annually laminated sediments composed of minerogenic
82 particles (clastic varves) formed when seasonal runoff carrying suspended sediment enters
83 a lake (Sturm, 1979) have the potential to produce long paleohydrological series. The direct
84 relationship between clastic varves and hydrological conditions makes this type of varve a
85 specific and powerful proxy for streamflow reconstructions. Clastic varves can provide, in
86 favourable settings, annually to seasonally resolved information about downstream
87 sediment transport from catchment area into lake basin depending on regional hydro-
88 climatic conditions (Lamoureux, 2000; Lamoureux et al., 2006; Tomkins et al., 2010;
89 Cuven et al., 2011; Kaufman et al., 2011; Schillereff et al., 2014; Amann et al., 2015;
90 Heideman et al., 2015; Zolitschka et al., 2015; Saarni et al., 2016; Czymzik et al., 2018).

91

92 Preliminary analysis of short sediment cores collected in Grand Lake, central Labrador,
93 revealed that this lake is an excellent candidate for the preservation of recent fluvial clastic
94 laminated sediment record (Zolitschka et al., 2015). The objectives of this paper are to: (1)
95 Confirm the annual character of the laminations record; (2) Establish the relation between
96 the physical parameters of laminations and local hydro-climatic conditions to examine the
97 potential proxy for hydrological reconstructions; (3) Reconstruct the hydrology of the last
98 160 years and compare its similarities and differences with Brigode et al. (2016) rainfall-
99 runoff modelling over the 1880-2011 period; and (4) Determine if there is a Labrador
100 regional streamflow signal recorded in Grand Lake laminated sediments.

101

102 **2. Regional setting**

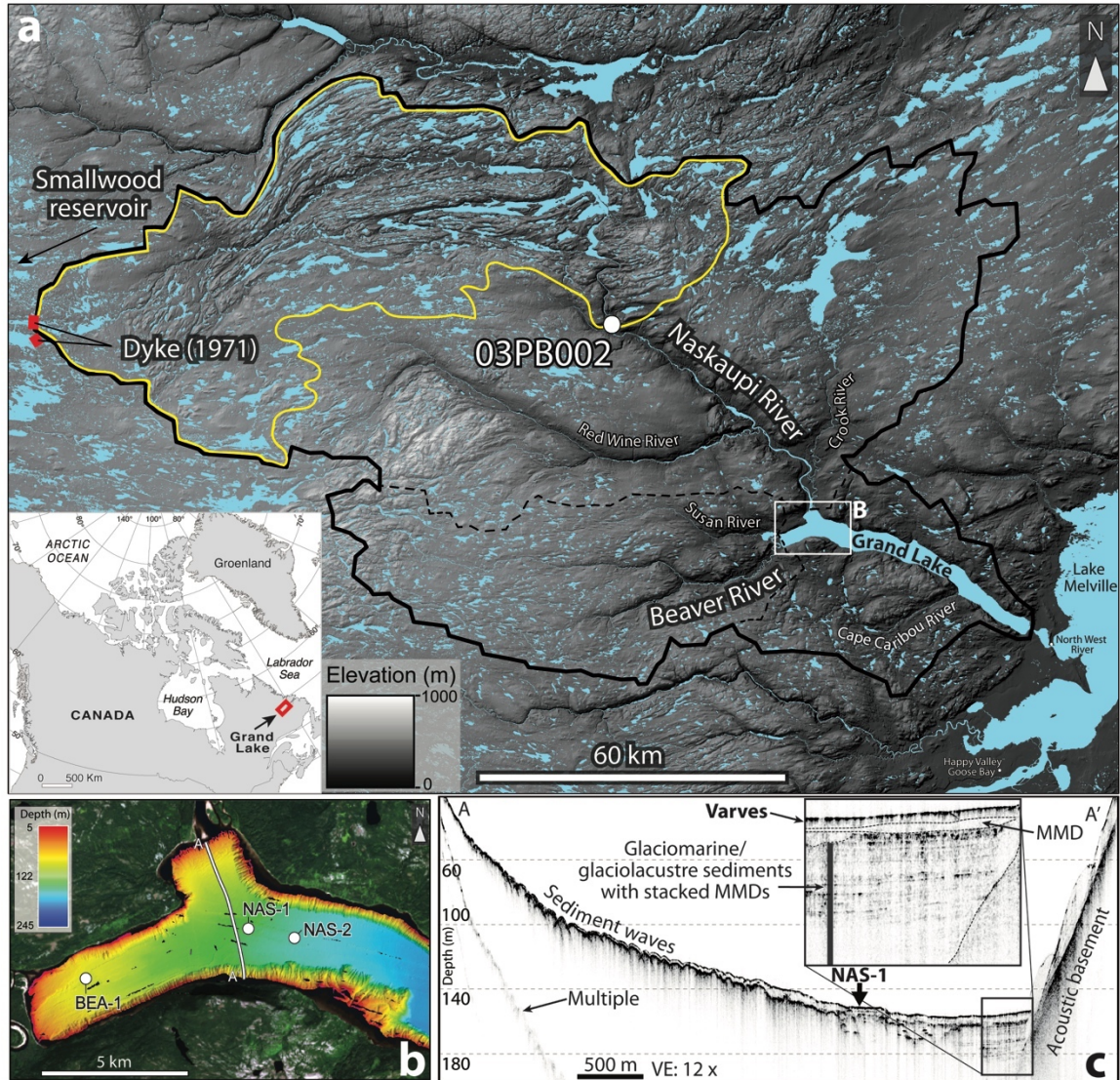
103 Grand Lake is a 245-m-deep (Trottier et al., 2020) elongated (60-km-long) fjord-lake
104 located in a valley connected to the Lake Melville graben in central Labrador
105 (53°41'25.58"N, 60°32'6.53"O, ~15 m above sea level) (Fig. 1). The region is part of the
106 Grenville structural province and is dominated by Precambrian granite, gneiss and acidic
107 intrusive rocks. Grand Lake watershed deglaciation began after ~8.2 cal ka BP (Trottier et
108 al., 2020). During deglaciation, marine limit reached an elevation of 120-150 m above
109 modern sea level and invaded further upstream in the modern fluvial valleys that are
110 connected to the lake (Fizthugh, 1973). This former glaciomarine/marine sedimentary fjord

111 basin has been glacio-isostatically uplifted and isolated by a morainic sill to become a deep
112 fjord-lake (Trottier et al., 2020). The regional geomorphology is characterized by glacially
113 sculpted bedrock exposures, glacial deposits consisting of till plateaus of various
114 elevations, glacial lineations, drumlins, kames, eskers and raised beaches (Fulton 1992).
115 Podzolic soils dominate, with inclusions of brunisols and wetlands.

116

117 Grand Lake is located in the High Boreal Forest ecoregion, one of the most temperate
118 climates in Labrador, hosting mixed forests dominated by productive, closed stands of
119 *Abies balsamea*, *Picea mariana*, *Betula papyrifera*, and *Populus tremuloides* (Riley et al.,
120 2013). This region is influenced by temperate continental (westerly and southwesterly
121 winds) and maritime (Labrador Current) conditions with cool humid summers (JJA) (~8.5
122 °C) and cold winters (DJFM) (~-13 °C). The Grand Lake watershed extends upstream over
123 the low subarctic Nipishish-Goose ecoregion, a broad bedrock plateau (<700 m.a.s.l.)
124 located on the west flank of the Lake Melville lowlands. Lichen-rich *Picea* woodlands with
125 open canopies predominate. With cooler summers and longer cold winters, this area is
126 slightly influenced by the Labrador Sea. Mean annual precipitation in the study region
127 ranges from 800 mm to 1 000 mm, with 400 cm to 500 cm of snowfall. The regional
128 hydrological regime typically exhibits winter low flow and spring freshet, followed by
129 summer flow recession (Fig. 2). Snowmelt in Grand Lake region takes place from April to
130 June (AMJ).

131



132

133 *Figure 1. (A) Location of Grand Lake watershed (black line) and its principal tributaries. The Naskaupi*
 134 *River hydrometric station (03PB002: white dot) covering an area of 4480 km² (yellow line). Location of the*
 135 *dykes constructed in 1971 to divert water from the Naskaupi River to the Smallwood reservoir hydroelectric*
 136 *system are also shown by the red bars. (B) High-resolution swath bathymetry (1-m resolution) of Grand Lake*
 137 *(Trottier et al., 2020) coupled with a Landsat image (USGS) and core site locations. The white line indicates*
 138 *the location of a typical 3.5 kHz subbottom profile (C) of the Naskaupi River delta (A-A') showing the*
 139 *approximate location of core NAS-1.*

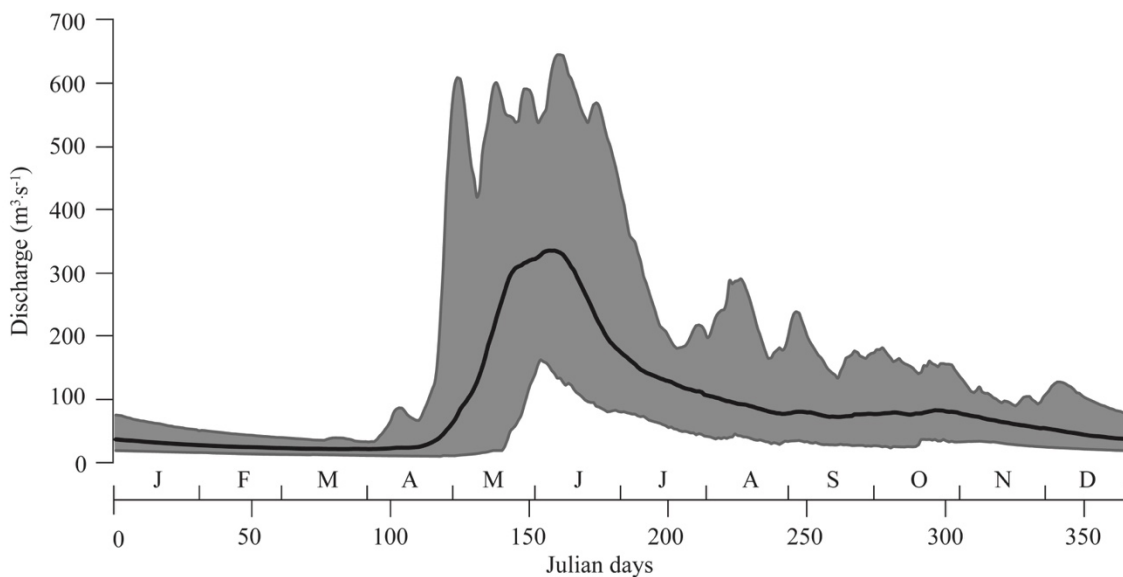
140 The main tributary of Grand Lake is the Naskaupi River located at the lake head (Fig. 1a).
 141 The downstream part of the Naskaupi River is fed by the Red Wine and the Crook rivers.
 142 The Beaver River is the secondary tributary of Grand Lake. Naskaupi and Beaver rivers
 143 structural valleys that connect to the Grand Lake Basin have a well-developed fluvial plain
 144 and a generally sinuous course that remobilize former deltaic systems and terraces
 145 composed of glaciomarine, marine, fluvio-glacial, lacustrine and modern fluvial deposits.

146 Upstream river terraces show mass movement scarps and are affected by gully and aeolian
147 activity. Grand Lake flows into a small tidal lake (Little Lake) and subsequently towards
148 Lake Melville. On 28 April 1971, by closing a system of dykes, the headwaters of Naskaupi
149 River watershed (Lake Michikamau) were diverted into the Churchill River hydropower
150 development (Fig. 1a). This diversion has reduced the drainage area of the Naskaupi River
151 from 23 310 km² to 12 691 km² (Anderson, 1985).

152

153 Hydroacoustic data were collected in Grand Lake in 2016 (Trottier et al., 2020). The swath
154 bathymetric imagery and 3.5 kHz subbottom profile show that the prodelta slopes present
155 well-defined sediment waves at the Naskaupi River mouth (Trottier et al., 2020; Fig. 1b).
156 The upper acoustic unit is composed of a high amplitude acoustic surface changing into
157 low amplitude acoustic parallel reflections (Fig. 1c), a type of acoustic facies which can be
158 associated with successive sedimentary layers of contrasting particle sizes (Gilbert and
159 Desloges, 2012).

160



161

162 *Figure 2. Observed mean daily discharges of the Naskaupi River (hydrometric station 03PB002) for the*
163 *1978-2012 period (black line). The gray zone represents the minimum and maximum observed discharges.*

164

165 **3. Methods**

166 **3.1 Sediment coring and processing**

167 Four short sediment cores (BEA-1, NAS-1A, NAS-1B and NAS-2) were collected using a
168 UWITEC percussion corer in March 2017 deployed from the lake ice cover. These cores
169 were collected in undisturbed areas according to the swath bathymetry and subbottom
170 profiling data (Trottier et al., 2020). Core BEA-1 was collected in the axis of the Beaver
171 River at a depth of 93 m. Core NAS-1 and NAS-2 were collected in the axis of the Naskaupi
172 River at a depth of 146 and 176 m, respectively (Fig. 1b). Site BEA-1 and NAS-1 are
173 located at the distal frontal slope of the Beaver and Naskaupi river deltas (fig. 1c); site
174 NAS-2 is located away from the Naskaupi River delta, at the beginning of the deep lake
175 basin. Duplicate cores of different lengths have been retrieved at each site to maximize
176 undisturbed sediment recovery. Following the extraction of each core, wet floral foam was
177 gently inserted through the top of the filled coring tube and slowly pushed towards the
178 sediment surface to seal and preserve the sediment-water interface. A plastic cap was then
179 installed on top of the foam to secure its position in contact with the intact sediment surface
180 and avoid disturbance during transport of the cores. The cores were scanned using a
181 Siemens SOMATOM Definition AS+ 128 medical CT-Scanner at the multidisciplinary
182 laboratory of CT-scan for non-medical use of the Institut National de la Recherche
183 Scientifique - Eau Terre Environnement (INRS-ETE). The CT-scan images allowed the
184 identification of sedimentary structures (i.e., laminated facies, perturbation and hiatus).
185 Expressed as CT-numbers or Hounsfield units (HU), X-Ray attenuation is a function of
186 density and the effective atomic number, and hence sensitive to contrasts in mineralogy,
187 grain size and sediment porosity (St-Onge et al., 2007). CT-numbers were extracted at a
188 resolution of 0.06 cm using the ImageJ software 2.0.0 (imagej.net). The cores were then
189 opened, described and photographed with a high-resolution line-scan camera mounted on
190 an ITRAX core scanner (RGB colour images; 50 µm-pixel size) at INRS-ETE.
191 Geochemical non-destructive X-Ray Fluorescence (XRF) analysis was performed on the
192 core half (30 kV and 30 mA). XRF elements profiles were used to visualize the structures
193 and boundaries of the laminations and estimate particle size variability in sediment cores
194 (Kylander et al., 2011; Cuvén et al., 2010; Croudace et al., 2006). Elements were

195 normalized by the total of count (cps) for each spectrum. Continuous XRF measurements
196 were also carried out on overlapping impregnated sediment blocks in order to superpose
197 element relative intensity profiles on thin-sections.

198 **3.2 Chronology and thickness measurement**

199 Surface sediments from cores BEA-1 and NAS-1A were dated with ^{137}Cs method (Appleby
200 and Oldfield 1978) using a high-resolution germanium diode gamma detector and
201 multichannel analyzer gamma counter. ^{137}Cs activity was used to identify sediment
202 deposited during 1963-1964 peak of nuclear tests and validate the annual character of the
203 layers. A sampling interval of 2 cm was used to approximately identify the depth at which
204 the ^{137}Cs peaks were located. Subsequently, a sampling interval of ± 0.5 cm was used to
205 sample each lamination for the period 1961-1965 to determine the exact ^{137}Cs peak location
206 (1963-1964). In order to establish a chronology for each core, detailed laminations counts
207 were executed on CT-scan images and high-resolution photographs using ImageJ 2.0.0 and
208 Adobe Illustrator CC softwares (Francus et al., 2002). As all of the core surface has been
209 well preserved, the first complete lamination below the sediment surface was considered
210 to represent the topmost year (i.e., 2016 CE). Chronology on each core was confirmed by
211 cross-correlation between thick laminations selected as distinctive marker layers along the
212 different sediment sequences (A to M; Fig. 4).

213

214 Thin-sections of sediments were sampled from cores BEA-1 (1856-2016), NAS-1A (1953-
215 2016), NAS-1B (1856-1952) and NAS-2 (1968-2016) (see Fig. 4 for thin-section location)
216 following Francus and Asikainen (2001) and Lamoureux (1994). Digital images of the thin-
217 sections were obtained using a transparency flatbed scanner at 2400 dpi resolution (1 pixel
218 = 10.6 μm) in plain light and were used to characterize lamination substructure. Lamination
219 counts and thickness measurements using a thin-section image analysis software developed
220 at INRS-ETE (Francus and Nobert 2007) were performed to duplicate and validate
221 previous chronologies established on CT-Scan images and high-resolution photographs.
222 Two counts were made from thin-section by the same observer (AGP). Total Varve
223 Thickness (TVT) and Detrital Layer Thickness (DLT) of each year of sedimentation were
224 measured from images of thin-sections. Lamination counts made on CT-scan images, high-

225 resolution photographs and thin-sections are identical while TVT measurements show
226 negligible difference ($R^2 = 0.96$; $p < 0.05$). The thickness measurements made from CT-
227 scan images and high-resolution photographs have been used to prolong the TVT series of
228 core NAS-2 from 1968 back to 1856. Continuous TVT measurements allowed the
229 establishment of high-resolution age-depth models for each site.

230 **3.3 Image and particle size analysis**

231 Using custom-made Image Analysis software (Francus and Nobert, 2007), regions of
232 interest (ROIs) were selected on the thin-section images. The software then automatically
233 yielded SEM images of the ROIs using a Zeiss Evo 50 scanning electron microscope
234 (SEM) in backscattered electron (BSE) mode. Eight-bit greyscale BSE images with a
235 resolution of 1024 x 768 pixels were obtained with an accelerating voltage of 20 kV, a tilt
236 angle of 6.1 and an 8.5 mm working distance with a pixel size of 1 μm . BSE images were
237 processed to obtain black and white images where clastic grains ($>3.5 \mu\text{m}$) and clay matrix
238 appeared black and white respectively (Francus, 1998).

239

240 Each sedimentary particle (an average of 2 225 particles per image) was measured
241 according to the methodology used by Lapointe et al. (2012), Francus et al. (2002) and
242 Francus and Karabanov (2000) in order to calculate particle size distribution on each ROI
243 image. Due to the thickness of the laminations, results from several ROI images were
244 merged to obtain measurements for each year of sedimentation, with an average of 4
245 images per lamination. Only clastic facies related to spring and summer discharges were
246 used for particle size analysis in order to exclude ice-rafted debris (μm to mm scale)
247 observed in the early spring layers (see Fig. 5 for details). The 99th percentile ($P99D_0$) of
248 the particle size distribution for each detrital layer was obtained from thin-sections
249 (Francus, 1998) for the last 160 years (1856-2016) for core BEA-1 and NAS-1, and for the
250 last 47 years (1968-2016) for core NAS-2, from 795, 717 and 132 BSE images respectively
251 (Fig. 4).

252

253 **3.4 Hydro-climatic variables**

254 Hydrological variables (Tab.1) were calculated from the time series of daily discharges
 255 recorded by the Naskaupi River hydrometric station over the 1978-2011 period (missing
 256 data from the years 1996, 1997 and 1998).

257

258 *Table 1. Hydro-climatic variables used in this paper*

Hydrological variable	Unit	Description
Q-max	m ³ /s	Annual maximum of daily discharges
Q-mean	m ³ /s	Mean annual discharge
Q-max-Jd	Julian days	Julian day at which the discharge reaches its maximum annual value
Rise-Time	Days	Number of days between the minimum winter flow and the maximum spring flow
Nb-Days-SupQ80	Days	Number of days with discharge greater than the 80 th daily percentile
Q-nival	mm	Nival runoff (April, May, June, July)
Snow-Win	mm	Winter snowfall (September to May)
Ptot-Annual	mm	Winter Snowfall + Summer rainfall
Ptot-Summ	mm	Summer rainfall (March to October)
Temp-Spring	°C	Average spring temperature (April, May, June)

259

260

261 The Naskaupi River hydrological variables have been compared with four other
 262 hydrometric station data available around the study region (Fig. 3a, Tab. 2), which are
 263 devoid of anthropogenic perturbations. Q-mean series from the five stations have been
 264 normalized for the common 1979–2011 period and averaged, to produce a Labrador region
 265 mean annual discharge series. This allows to extend instrumental data series for the period
 266 1969 to 2011, and fill in data for the missing years. The Labrador hydrometric station data
 267 used in this study come from a Government of Canada website (<https://wateroffice.ec.gc.ca>
 268 05/2018).

269

270 *Table 2. Description of hydrometric stations used in this study*

Hydrometric station	ID	Area (km ²)	Location (N,W)	Recording period
Ugjoktok River	03NF001	7570	55° 14' 02", 61° 18' 06"	1979-2011
Naskaupi River	03PB002	4480	54° 07' 54", 61° 25' 36"	1978-2011
Minipi River	03OE003	2330	52° 36' 45", 61° 11' 07"	1979-2011
Little Mecatina River	02XA003	4540	52° 13' 47", 61° 19' 01"	1979-2011
Eagle River	03QC001	10 900	53° 32' 03", 57° 29' 37"	1969-2011

271

272

273 **3.5 Varve physical parameters and hydrological variables**

274 A simple linear regression model was used to fit the DLT and P99D₀ series with local
275 (1978-2011) and regional (1969–2011) instrumental series and reconstructed hydrological
276 variables (Q-mean, Q-max) back to 1856. Model calibration was performed using a
277 twofold cross-validation technique over the instrumental period. Root mean squared errors
278 (RMSE) and coefficient of determination (R^2) were calculated for calibration periods,
279 while average reduction of error (RE) and average coefficient of efficiency (CE) were
280 calculated to evaluate reconstruction skills (Briffa et al. 1988, Cook et al., 1999). The RE
281 and CE of the verification periods must be > 0 to validate the model skills. Statistical
282 analysis was realized using the treeclim package (Zang and Biondi, 2015) in the R-project
283 environment (R Core Team, 2019, <http://www.r-project.org/>).

284

285 **3.6 Hydro-climatic reconstruction based on rainfall-runoff modelling**

286 The applied reconstruction method is based on rainfall-runoff modelling. Firstly, it aims at
287 producing, for the Naskaupi River hydrometric station catchment (Fig. 1a), daily climatic
288 time series using a historical reanalysis of global geopotential height fields extracted over
289 the studied region for a given time period (here 1880-2011). Secondly, the produced
290 climatic series are used as inputs to a rainfall–runoff model previously calibrated on the
291 studied catchment in order to obtain daily streamflow time series. The reconstruction
292 method is fully described in Brigode et al. (2016) and was recently applied over
293 southeastern Canada catchments in Dinis et al. (2019). It is summarized in the following
294 paragraphs.

295

296 The available observed hydro-climatic series for the Naskaupi River hydrometric station
297 catchment have been aggregated at the catchment scale. Climatic series (daily air
298 temperature and precipitation) have been extracted from the CANOPEX dataset (Arsenault
299 et al., 2016), built using Environment Canada weather stations and Thiessen polygons to
300 calculate climatic series at the catchment scale. Daily air temperature series have been used
301 for calculating daily potential evapotranspiration at the catchment scale, using the Oudin
302 et al. (2005) formula designed for rainfall-runoff modelling.

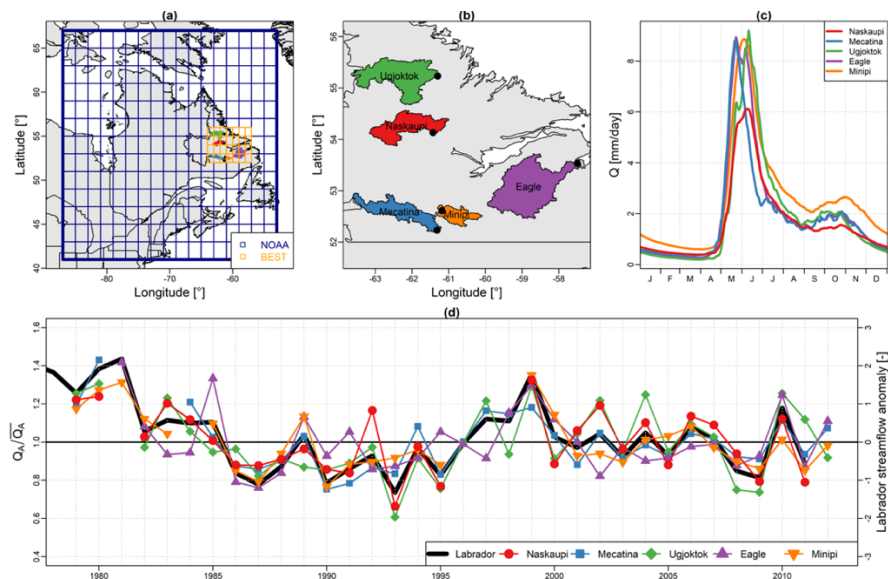
303

304 These daily series have been used for calibrating the GR4J rainfall-runoff model (Perrin et al., 2003) and its snow accumulation and melting module, CemaNeige (Valéry et al., 2014a), using the airGR package (Coron et al., 2017). This combination of GR4J and CemaNeige (hereafter denoted CemaNeigeGR4J) has been recently applied over eastern Canada catchments and showed good modelling performances (e.g., Seiller et al., 2012; Valéry et al., 2014b, Brigode et al., 2016). CemaNeigeGR4J has been calibrated on the recorded period of the Naskaupi River hydrometric station catchment using the Kling and Gupta efficiency criterion (Gupta et al., 2009) as objective function.

312

313 Then, the observed climatic series have been resampled over the 1880-2011 period, based on both season and similarity of geopotential height fields (Kuentz et al., 2015). The resampling is performed by calculating Teweles and Wobus (1954) distances between four geopotential height fields: (i) 1000 hPa at 0 h, (ii) 1000 hPa at 24 h, (iii) 500 hPa at 0 h, and (iv) 500 hPa at 24 h. The NOAA 20th Century Reanalysis ensemble (Compo et al., 2011, hereafter denoted 20CR) has been used as a source of geopotential height fields (Fig. 3b).

320



321

322 *Figure 3. (a) Dataset used for the hydro-climatic reconstruction based on rainfall-runoff modelling: the*
 323 *extension of the 20CR grid used is shown in blue, while the BEST grid used is highlighted in orange. (b)*
 324 *Spatial distribution of hydrometric stations used in this study (black dots) and their catchment area. (c)*
 325 *Observed mean daily discharges of each hydrometric station for the 1978-2012 period. (d) Labrador*
 326 *streamflow anomaly and the Labrador region mean annual discharge series (thick black line).*

327 As in Brigode et al. (2016), the resampled series of air temperature have been corrected at
328 the catchment scale using a regression model calibrated with the Berkeley Earth Surface
329 Temperature analysis (Rohde et al., 2013, hereafter denoted BEST). BEST is a gridded air
330 temperature product starting in 1880 at the daily timestep (Fig. 3b).

331

332 Finally, the daily climatic series are used as inputs to the CemaNeigeGR4J model in order
333 to obtain daily streamflow time series on the same 1880-2011 period. Thus, the outputs of
334 the hydro-climatic reconstruction are an ensemble of daily meteorological series (air
335 temperature, potential evapotranspiration and precipitation) and an ensemble of daily
336 streamflow series.

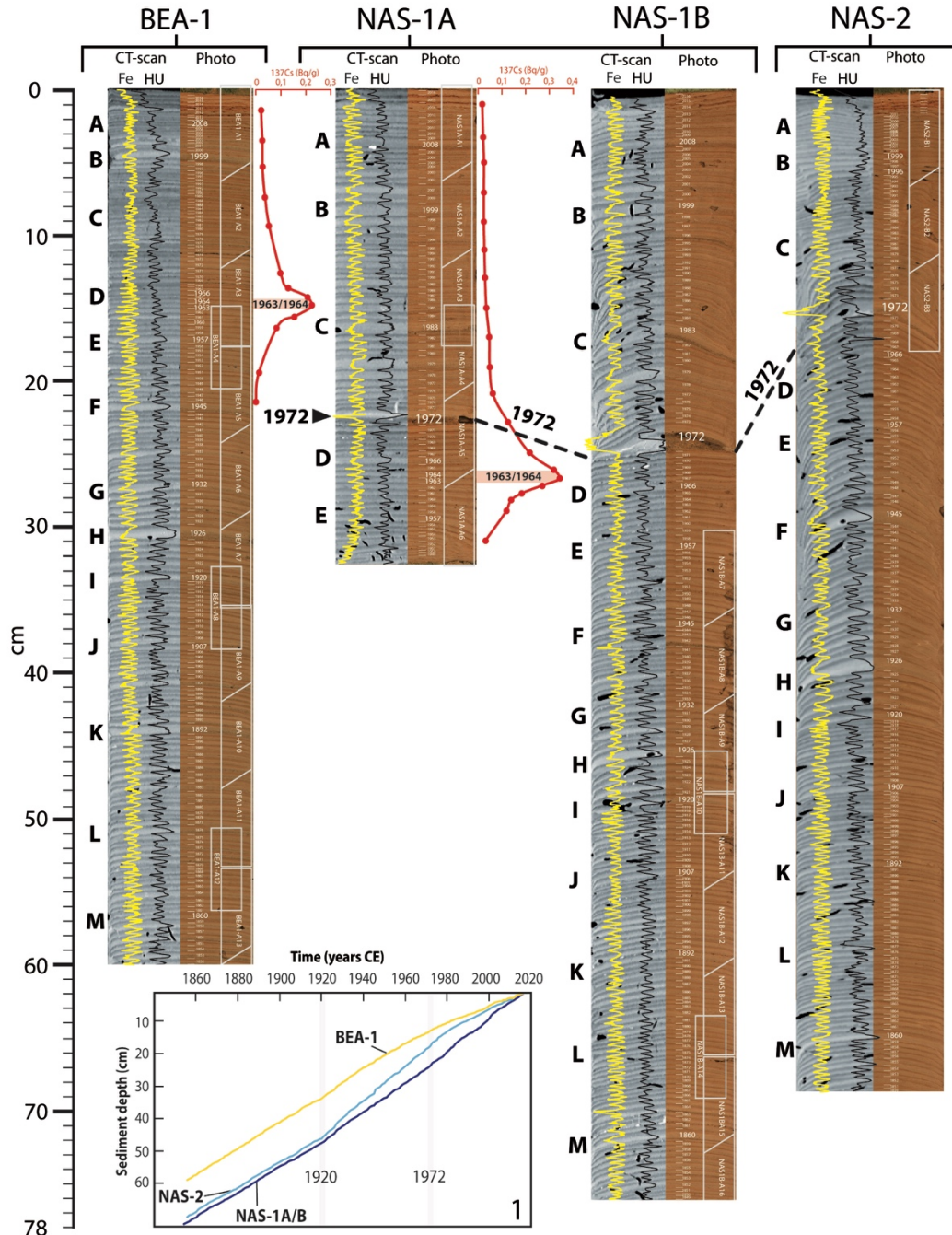
337

338 **4. Results**

339 **4.1 Lamination characterization**

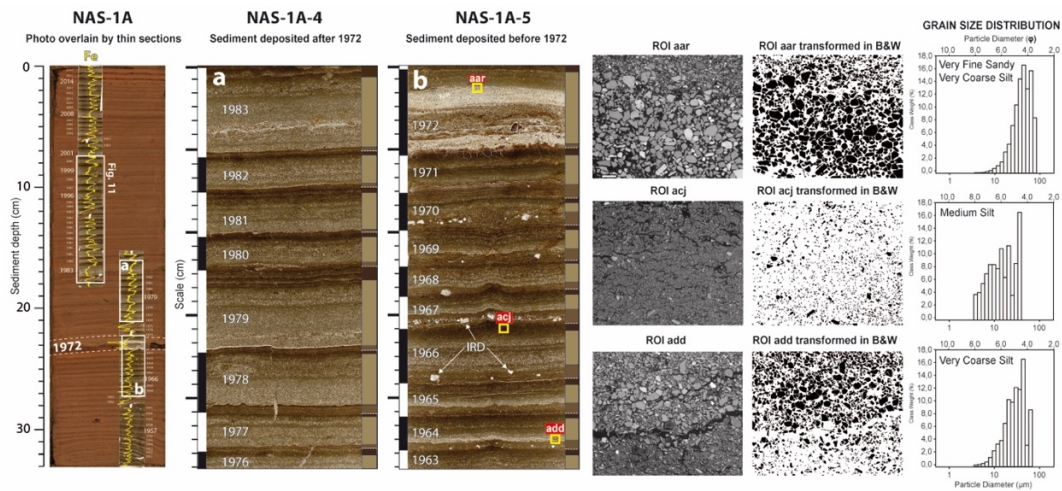
340 Sediment retrieved at the head of Grand Lake (Fig. 4), consist of dark grayish to dark
341 yellowish brown (Munsell colour: 10YR-4/2 to 10YR-4/4) laminated minerogenic
342 material, interpreted as clastic lamination of fluvial origin. Lamination structure can be
343 divided in 3 seasonal layers (Fig. 5) based on their stratigraphic position and microfacies.
344 Annual sedimentation starts with a layer composed of silt and clay sediment matrix which
345 sometimes contains ice-rafted debris (μm to mm scale) interpreted as an early spring layer.
346 The major lamination component is a spring and summer/autumn detrital layer. Its thick
347 basal part is mostly poorly sorted, graded and composed of coarse minerogenic grains
348 comprising fine sand and silts ($< 150 \mu\text{m}$) with some redeposited cohesive sediment clasts
349 eroded from the underlying early spring layer. This detrital layer has a sharp lower
350 boundary. The upper part of the detrital layer consists of a finer detrital grain matrix
351 containing thin visually coarser intercalated sub-layers in $\sim 75\%$ of the laminations. The
352 allochthonous lithoclastic materials which compose the detrital layers are associated with
353 higher density values (Fig. 4) and an increase in the relative intensity of elements Sr and
354 Ca (Zolitschka et al., 2015). Few organic debris and charcoal fragments are observed
355 throughout the detrital layers. The third topmost lamination layer is formed by a fine to
356 medium silty layer with abundant clay rich in Fe and interpreted as an autumn and winter
357 layer, also known as a clay cap (Zolitschka et al., 2015). The Fe peak values in autumn and

358 winter layers, are hence used to determine the upper lamination boundary (Fig. 4)
 359 (Zolitschka et al., 2015) as previously performed in other varved sequences (Cuven et al.,
 360 2010; Saarni et al., 2016).



361
 362 Figure 4. Varve counts made on (left) CT-scan and (right) high resolution images from core BEA-1, NAS-
 363 1A/B and NAS-2. Distinctive marker layers are identified by letters A to M. The 1972 marker layer is outlined
 364 by the thick dark gray line. Fe relative intensity and density (HU) profile represented by the yellow and black
 365 line respectively, show rhythmic laminations. The activity profile of ^{137}Cs in core BEA-1, NAS-1A is shown
 366 by the red line. Approximate thin-section locations are outlined by white boxes. The age-depth model of the
 367 3 cores is also presented (Box. 1). See Fig. 1b for core locations.

368 The lamination deposited in 1972 from sites in the axis of the Naskaupi River (NAS-1; Fig.
 369 5b and NAS-2; Fig. 4), present a thick (8.2 mm) and coarse (67.8 μm) detrital layer
 370 composed of very fine sandy and very coarse silt (Fig. 5b) representing the highest particle
 371 size measured in all sequences. Furthermore, there is a difference in lamination physical
 372 parameters and microfacies deposited before and after the 1972 marker bed, especially in
 373 core NAS-1, the proximal site from the Naskaupi River mouth. Laminations deposited
 374 prior 1972 have a well-developed substructure relatively constant among each annual
 375 lamination (Fig. 5b). The early spring layer of the pre-1972 laminations is thicker and more
 376 clearly visible. Conversely, the detrital layer of laminations post-1972 is thicker, while the
 377 early spring layer is more difficult to discern and contributes less to the TVT (Fig. 5a). The
 378 mean contribution of the early spring layer and autumn and winter layer to the total
 379 lamination thickness is 35% for the pre- and 52% for the post-1972 intervals. The early
 380 spring layer in lamination post-1971 from sites NAS-1 and NAS-2 no longer contains
 381 isolated coarse debris. The changes in lamination facies are less noticeable in core NAS-2,
 382 which was sampled further away from the Naskaupi River mouth. The 1972 marker bed
 383 and related facies changes are not found at the Beaver River mouth site BEA-1.
 384



385
 386 *Figure 5. (Left) Photo of core NAS-1A overlain by thin-section image and Fe relative intensity profile (yellow*
 387 *lines). The 1972 marker layer is outlined by the white dashed lines. Thin-section images showing sedimentary*
 388 *structure of varves deposited (B) before and (A) after the 1972 marker bed. Varve boundaries are represented*
 389 *by the vertical black and white bars. Varve layers are delimited by the medium brown (early spring layer),*
 390 *pale brown (detrital layer) and dark brown (autumn and winter layer) bars. Typical Ice-Rafted Debris (IRD)*
 391 *are shown by the white arrows on the b panel. (Right) BSE images of three ROIs transformed in B&W and*
 392 *their associated particle size distribution (aar: the 1972 marker layer; acj: a typical autumn and winter*
 393 *layer; add: the base of a typical detrital layer) (see yellow squares on the b panel for ROIs location).*

394 **4.2 Varve chronology**

395 The laminated sequences chronologies are consistent with the Cesium-137 main peaks
396 corresponding to the highest atmospheric nuclear testing period (1963-1964 CE) (Appleby,
397 2001). Peaks are found at 14-14.5 cm (BEA-1) and 26.5-27 cm (NAS-1A) depth (Fig. 4)
398 and perfectly match the lamination counts in both cores, confirming the varve assumption.
399 The presence of the distinct 1972 marker layer at this chronostratigraphic position in the
400 varve sequence which coincides with the occurrence of the Naskaupi River diversion that
401 took place in April 1971 (see section 5.2 for details) supports the reliability of the
402 constructed chronologies.

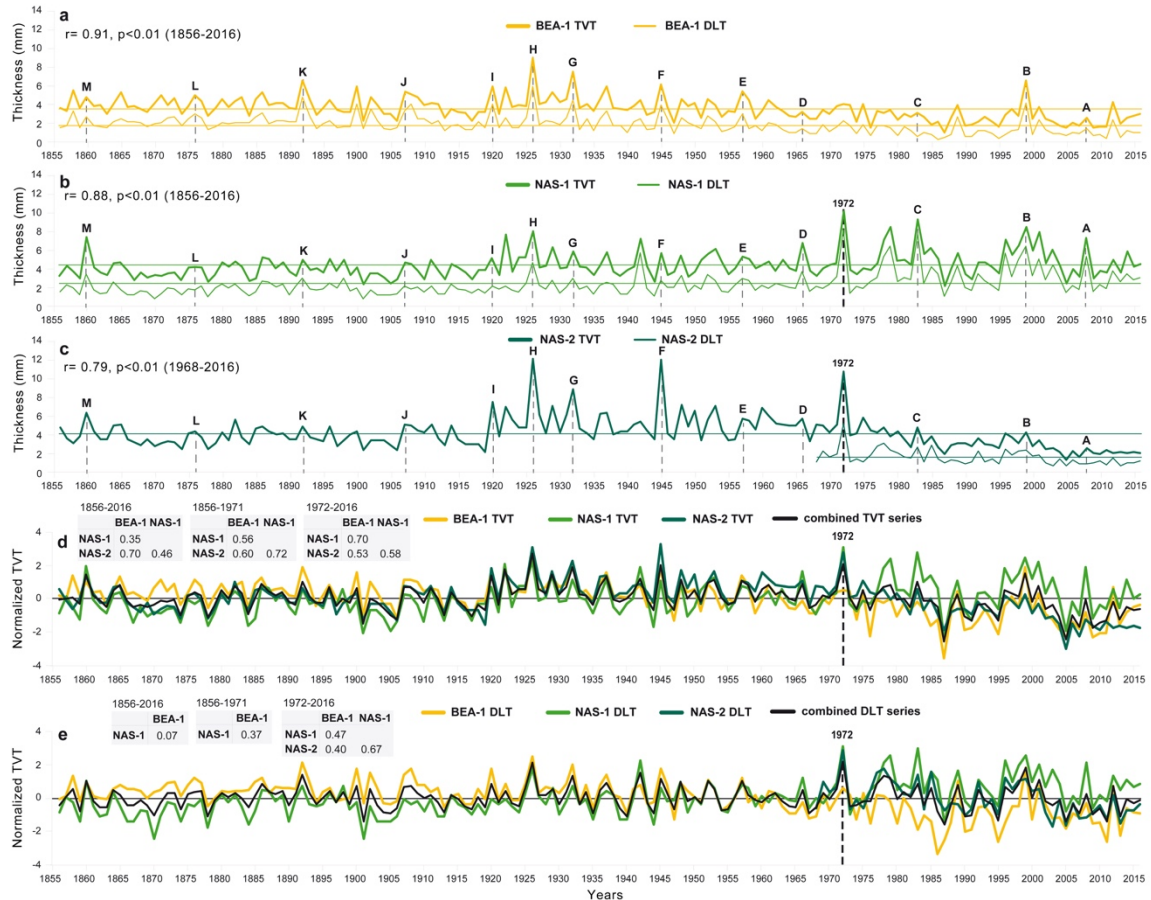
403

404 Independent varve chronologies were established from sediment cores BEA-1, NAS-1 and
405 NAS-2 (Fig. 4). A total of 160 varves were counted at each site, covering the 1856-2016
406 period. The thickness and the good quality of the well-preserved varve structures allowed
407 a robust age-model reproducible among cores to be constructed. Despite the distance
408 between the coring sites (1 to 5 km) and the two different sediment sources (Naskaupi and
409 Beaver River) (Fig. 1b), there is no varve count difference between the selected thick
410 marker layers (A to M; Fig. 4) among cores. The few counting difficulties occur within
411 varve years 1952-1953, 1935-1934, 1918-1919, as it contains ambiguous coarse non-
412 annual intercalated sub-layers with intermediate clay cap that can be interpreted as one year
413 of sedimentation. Both varve counts performed on thin-sections show a low overall
414 counting error ($\pm 1.8\%$) which demonstrated the precision and accuracy of the varve
415 sequences chronology. The age-depth models (Fig. 4, Box. 1) show changes in sediment
416 accumulation rates (thickness) among cores in 1920 and 1972.

417 **4.3 Thickness and particle size measurements**

418 The TVTs from core BEA-1, NAS-1 and NAS-2 vary between 0.9 and 12.9 mm, with an
419 average thickness of 4.09 mm (Fig. 6a, b, c, Supplements Fig. S1 and Tab. S1). The DLTs
420 vary between 0.3 and 8.3 mm, with an average thickness of 1.9 mm (Fig. 6a, b, c,
421 Supplements Fig. S2 and Tab. S2). There are significant strong positive correlations
422 between TVT and DLT for each core ($r = 0.79$ to 0.91 ; $p < 0.01$). A step in the TVT is
423 observable in the early 1920s at the three sites (Fig. 6a, b, c), especially in core NAS-2,

424 which recorded their highest values (12.9 mm) during the 1920-1972 period (Fig. 6c).
425 Since the 1920s, there is a statistically significant decreasing trend in TVTs and DLTs in
426 core BEA-1 (Fig. 6a). Thickness data from the three sites have been normalized and
427 averaged to produce combined TVT and DLT series (Fig. 6d, e). From 1920 to 1972,
428 combined TVT and DLT series show a statistically significant downward trend, despite an
429 increase in years associated with high thickness values. Overall, TVT and DLT vary
430 similarly in time between sites during the 1856-1971 period (Fig. 6d, e). However, after
431 1972, TVT and DLT series are more diverging. From 1972 to 2016, there is a statistically
432 significant decreasing trend in TVT and DLT in cores NAS-2 (Fig. 6c), and the amplitude
433 of their variability tends to diminish. For core NAS-1 (Fig. 6b), post-1971 period is
434 associated with higher thickness values. Core NAS-1 has recorded a slight TVT and DLT
435 decrease for the 1972-2016 period, but unlike the other cores, the variability tends to
436 increase. The TVT and DLT are overall finer in the distal core NAS-2 compared to the
437 more proximal core NAS-1 (Fig. 4, Box. 1, Supplements Tab. S1, S2).
438



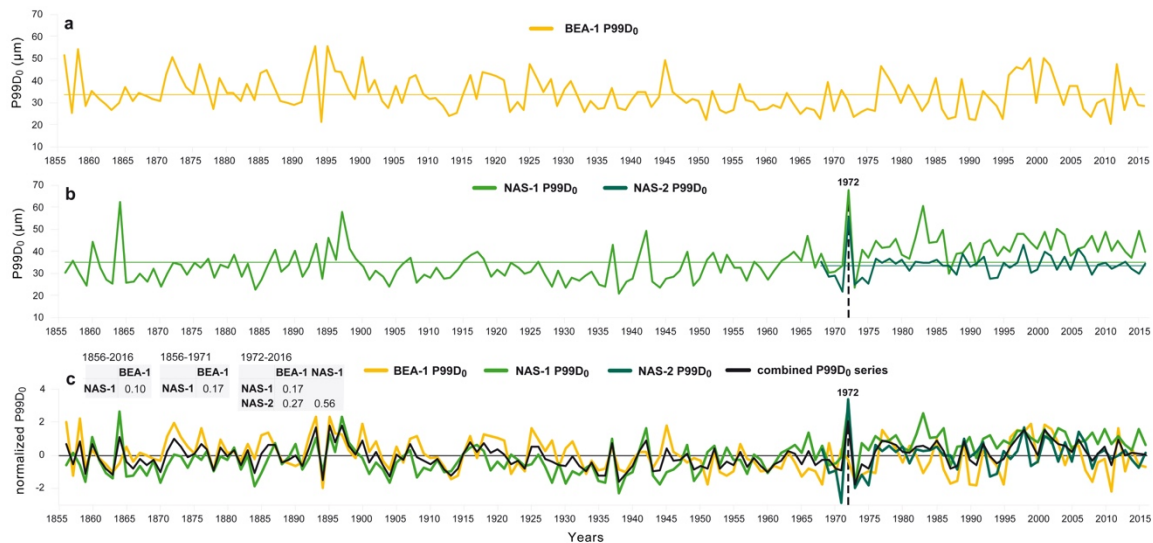
439

440 *Figure 6. Total Varve Thickness (TVT; thick line) and Detrital Layer Thickness (DLT; thin line) time series*
 441 *of core (a) BEA-1, (b) NAS-1 and (c) NAS-2. Normalized (d) TVT and (e) DLT series and the combined series*
 442 *(mean of the normalized data from the 3 sites). Pearson correlation coefficients between TVT and DLT for*
 443 *the 1856-2016, 1856-1971 and 1973-2016 periods are shown. The selected marker layers are identified by*
 444 *letters A to M and the 1972 marker layer is outlined by the thick black dashed line.*

445 The P99D₀ of cores BEA-1, NAS-1 and NAS-2 vary between 20 and 67.8 μm, with an
 446 average value of 34.3 μm (Fig. 7, Supplements Fig. S3 and Tab. S3). The grain size is finer
 447 in core NAS-2 compared to core NAS-1. Particle size data from the three sites have been
 448 normalized and averaged to produce combined P99D₀ series (Fig. 7c). The combined
 449 P99D₀ series show a slight coarsening trend towards the end of the 19th century. From 1900
 450 to 1971, P99D₀ values are generally below average. The 1972 marker layer of core NAS-
 451 1 presented the maximum P99D₀ values (Fig. 7b). After 1972, there is an increase of P99D₀
 452 values in core NAS-1, where a step is observable. Pre-1971 varves in core NAS-1 have a
 453 mean P99D₀ of 32,47 μm compared to 42,91 μm for the 1972-2016 period.

454

455 There is weak to moderate positive correlation between TVT and P99D₀ from a same core
 456 (BEA-1: $r = 0.41$ $p < 0.01$; NAS-1: $r = 0.52$ $p < 0.01$; NAS-2: $r = 0.27$, $p < 0.05$). The
 457 correlation between DLT with P99D₀ is stronger (BEA-1: $r = 0.49$ $p < 0.01$; NAS-1: $r =$
 458 0.65 $p < 0.01$; NAS-2: $r = 0.49$, $p < 0.01$). Thick varves are more likely to have high grain
 459 size values. However, these correlations show that TVT, DLT and P99D₀ remain
 460 independent variables and can both reveal different hydrological information.
 461



462
 463 *Figure 7. P99D₀ time series of cores (a) BEA-1, (b) NAS-1 (1856-2016) and NAS-2 (1968-2016). (c)*
 464 *Normalized P99D₀ series and the combined series (mean of the normalized data from the 3 sites). The 1972*
 465 *marker layer is outlined by the black dashed line. Pearson correlation coefficients between P99D₀ series for*
 466 *the 1856-2016 and 1968-2016 periods are shown.*

467 4.5 Relation between varve series and instrumental record

468 4.5.1 Naskaupi River

469 To examine how the physical parameters of the varves are related to local hydroclimate
 470 and to demonstrate their potential for hydrological reconstruction, sediment parameters
 471 (TVT, DLT and P99D₀) of each core were systematically compared to hydrological
 472 variables (Tab. 1). TVT, DLT and P99D₀ series from the three coring sites show significant
 473 positive correlations with the Q-mean and Q-max extracted from the Naskaupi River
 474 hydrometric station (03PB002) data on the 1978-2011 period (n=31) (Tab. 3). The TVT
 475 and DLT of cores BEA-1 and NAS-2 show stronger correlation with Q-mean, while TVT
 476 and DLT of cores NAS-1 have a better relation with Q-max. There is a significant negative
 477 correlation between P99D₀ of core NAS-1 and Q-max-Jd ($r = -0.38$) and Rise-Time
 478 ($r = -0.47$). Sediment parameters also present significant positive correlations with Q-

479 Nival ($r = 0.32$ to 0.61), Snow-Win ($r = 0.47$ to 0.61) and Nb-days-SupQ80 ($> 125 \text{ m}^3 \cdot \text{s}^{-1}$)
480 ($r = 0.44$ to 0.62). Moreover, the maximum particle size series of core NAS-1 show
481 significant ($p = 0.02$) positive correlations with the average spring temperature ($r = 0.40$;
482 not shown in Tab. 3). Combined DLT and P99D₀ series (Fig. 6d, e; 7c) yields the strongest
483 correlations in our dataset ($r = 0.68$ and 0.75 ; Tab. 3) and have been used to reconstruct
484 Naskaupi River Q-mean and Q-max respectively (Fig. 8).

485

486 *4.5.2 Labrador region*

487 To determine if there is a regional hydrological signal in Labrador and whether the Grand
488 Lake varved sedimentary sequence has recorded this signal, the Naskaupi River hydro-
489 climatic variables were compared with other Labrador hydrometric stations (Tab. 2).
490 Despite specific local geomorphological and climatic conditions, strong similarities exist
491 between observed mean daily discharges (Fig. 3c) and annual streamflow (Fig. 3d)
492 recorded by hydrometric stations in Labrador for the 1978-2011 period. The shape of the
493 five annual regimes shows similar characteristics (i.e. flood-timing, strength, duration,
494 snowmelt and rainfall response). The instrumental Naskaupi River mean annual discharge
495 series data show significant ($p < 0.01$, Supplements Tab. S5) positive correlations with
496 other hydrometric stations (Ugjoctok: $r = 0.84$; Minipi: $r = 0.70$; Little Mecatina: $r = 0.73$;
497 Eagle: $r = 0.49$). Hydrological conditions in the Naskaupi river region is thus representative
498 of a broader region of Labrador. Therefore, the combined DLT series (without the NAS-1
499 1978-2016 period) has been used to reconstruct the Labrador region mean annual discharge
500 series (Fig. 9).

501

502 Table 3. Matrix of correlation coefficients (Pearson r) of the hydro-climatic variables defined in
 503 Tab. 1 with Total Varve Thickness (TVT), Detrital Layer Thickness (DLT) and particle size (P99D₀)
 504 on the instrumental period (1978-2011; $n=31$) for each core. Correlations between the hydro-
 505 climatic variables and the combined TVT, DLT and P99D₀ series (normalized and averaged varve
 506 parameters of cores BEA, NAS-1 and NAS-2) are also present. Correlations in boldface are
 507 significant at $p < 0.05$ (Supplements Tab. S4). Correlations marked by an asterisk were used for the
 508 final Q-mean and Q-max reconstructions.

		Hydroclimatic variables of station 03PB002						
Core BEA-1		Q-mean	Q-max	Q-max-Jd	Rise-Time	Nb-days-supQ80	Q-nival	Snow-Win
TVT		0.53	0.46	-0.19	-0.06	0.54	0.41	0.47
DLT		0.54	0.38	-0.01	0.22	0.44	0.32	0.29
P99D ₀		0.56	0.56	-0.05	0.17	0.34	0.40	0.24
Core NAS-1		Q-mean	Q-max	Q-max-Jd	Rise-Time	Nb-days-supQ80	Q-nival	Snow-Win
Sediment parameters	TVT	0.52	0.64	-0.31	-0.26	0.55	0.56	0.55
	DLT	0.53	0.67	-0.31	-0.27	0.53	0.54	0.50
	P99D ₀	0.19	0.60	-0.38	-0.47	0.26	0.40	0.30
Core NAS-2		Q-mean	Q-max	Q-max-Jd	Rise-Time	Nb-days-supQ80	Q-nival	Snow-Win
TVT		0.49	0.45	0.04	-0.24	0.56	0.47	0.61
DLT		0.62	0.57	0.07	-0.13	0.59	0.61	0.60
P99D ₀		0.39	0.43	0.19	0.26	0.31	0.40	0.11
combined series		Q-mean	Q-max	Q-max-Jd	Rise-Time	Nb-days-supQ80	Q-nival	Snow-Win
TVT		0.56	0.58	-0.19	-0.20	0.60	0.53	0.59
DLT		0.68*	0.65	-0.11	-0.07	0.62	0.58	0.54
P99D ₀		0.59	0.75*	-0.09	0.05	0.43	0.56	0.23

509

510 4.6 Hydrological reconstructions using varve parameters

511 4.6.1 Naskaupi River Q-mean and Q-max

512 The Naskaupi River mean and maximum annual discharges (Q-mean and Q-max) were
 513 reconstructed using DLT and P99D₀ series for the 1856–2016 period. The reconstructions
 514 were performed using single-core data, combined DLT and P99D₀ series and other
 515 combinations of core data, in order to propose the most relevant reconstructions
 516 (Supplements Fig. S4, S5). The observations and the reconstructed Q-mean and Q-max
 517 extracted from the different series over the 1978-2011 period are consistent. Despite
 518 differences, all reconstructions tested using different sources of sedimentological data
 519 generally share common interannual and longer-term variability.

520

521 Excluding the 1972-2016 measurements from NAS-1 from the combined series for
 522 reconstructions was also tested to remove the likely anthropogenic impact on sedimentation
 523 during this period. The combined DLT series without the 1972-2016 period presents a

524 slightly better fit with the instrumental data (lowest RMSE and the most-significant and
525 highest R^2 , Supplements Tab. S6). The model calibrations based on a twofold cross-
526 validation reveal that this DLT series has better overall predictive capacity to reconstructed
527 Q-mean (Supplements Tab. S7). The 1972-2016 period of core NAS-1 was then excluded
528 from the combined DLT series used to perform the best reconstruction of Naskaupi River
529 Q-mean presented in Fig. 8a. However, significantly stronger calibration and validation
530 statistical results were obtained by keeping this period in the combined P99D₀ series used
531 to reconstruct Naskaupi River Q-max (Fig. 8b, Supplements Tab. S8, S9). The varve of
532 year 1972 is considered as an outlier that originated from anthropogenic impacts, and thus
533 was not included in all reconstructions.

534

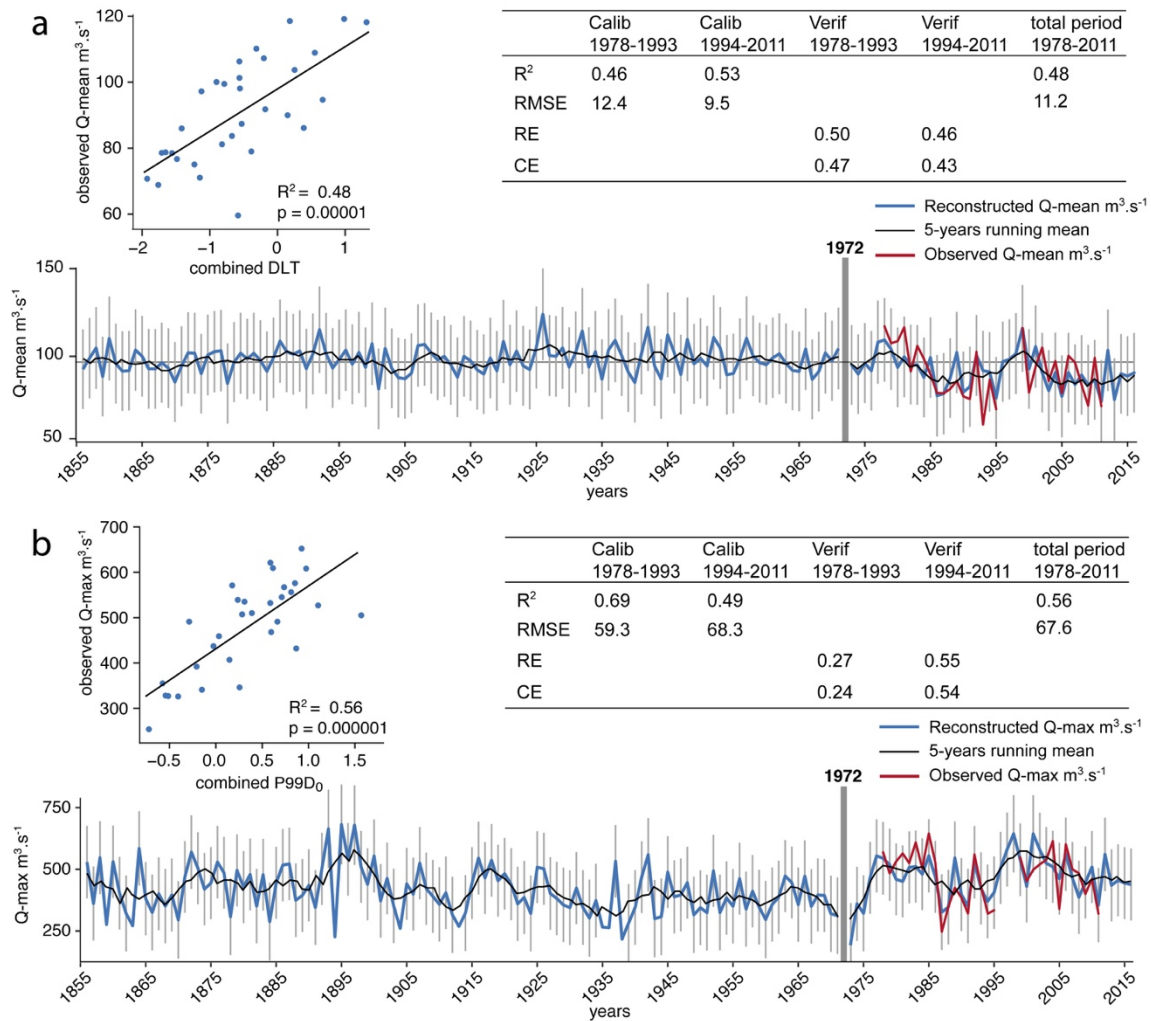
535 The reconstructed Naskaupi River Q-mean from combined DLT series varies between 73
536 and $126 \text{ m}^3 \cdot \text{s}^{-1}$, with an average of $96 \text{ m}^3 \cdot \text{s}^{-1}$ (Fig. 8a), and remains relatively stable from
537 1856 to 1920, mainly near average. Several years with high Q-mean occurred during the
538 1920-1960 period. A statistically significant downward trend of the Q-mean is observed
539 over the last 90 years. Recently, high Q-mean periods are observed from 1976 to 1985 and
540 1996 to 2002 and lower Q-mean periods from 1986 to 1995 and 2003 to 2016. The
541 reconstructed Naskaupi Q-max from combined P99D₀ series varies between 192 and 681
542 $\text{m}^3 \cdot \text{s}^{-1}$, with an average of $426 \text{ m}^3 \cdot \text{s}^{-1}$ (Fig. 8b). There is a slight upward trend in Q-max at
543 the end of the 19th century. The 1900-1971 period is characterized by a Q-max generally
544 below average. Three periods of high Q-max are observed from 1887 to 1900, 1976 to
545 1986 and 1995 to 2008 (Fig. 8b).

546

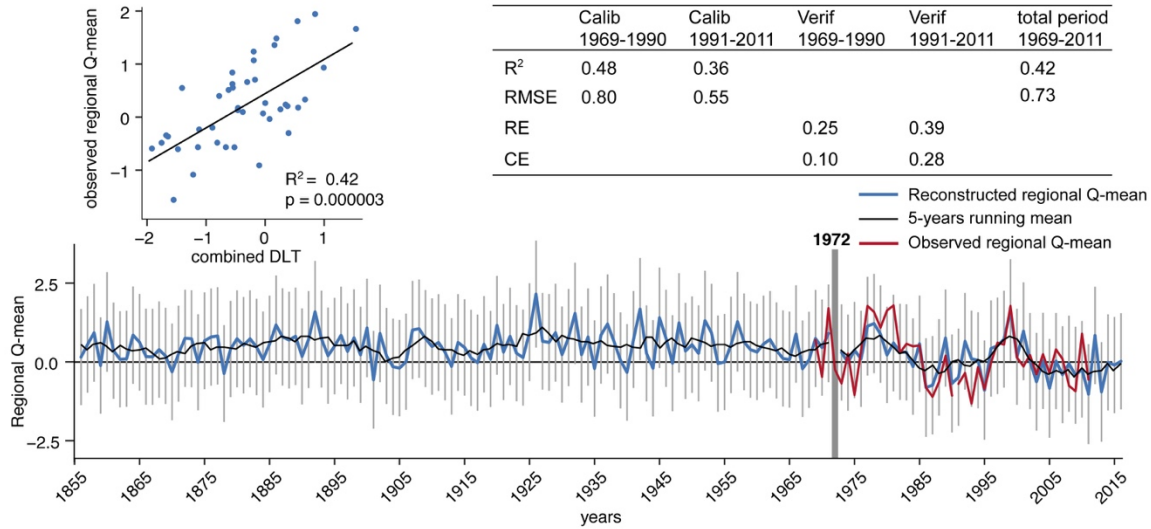
547 *4.6.2 Labrador region Q-mean*

548 The consistency between combined DLT series and the observed Labrador region Q-mean
549 series (Fig. 9), based on the discharge variability of five watersheds of different size and
550 location, demonstrates that the Grand Lake varved sequence contains a regional signal. The
551 best reconstruction of Labrador region mean annual discharges is the one performed using
552 the combined DLT series without the NAS-1 1972-2016 period. This reconstruction
553 demonstrates the best predictive capacity (RE and CE must be > 0 to validate the model

554 skills, Supplements Tab. S10, S11). The regional Q-mean reconstruction for the 1856–
 555 2016 period is presented in Fig. 9.
 556



557
 558 *Figure 8. Naskaupi River (a) Q-mean and (b) Q-max reconstructed from combined DLT (Without the NAS-*
 559 *I 1978-2016 period) and P99D₀ series respectively, for the 1856–2016 period (blue line), with 5-year*
 560 *moving average (black line). Error bars represent the 95% confidence interval. Observed Q-mean and Q-*
 561 *max are also shown for the 1978-2011 period (red line).*



562
563
564
565
566

Figure 9. Labrador region Q-mean reconstructed from combined DLT series (without the NAS-1 1972-2016 period) for the 1856–2016 period (blue line), with 5-year moving average (black line). Error bars represent the 95% confidence interval. Observed Labrador region Q-mean series is also shown for the 1969-2011 period (red line).

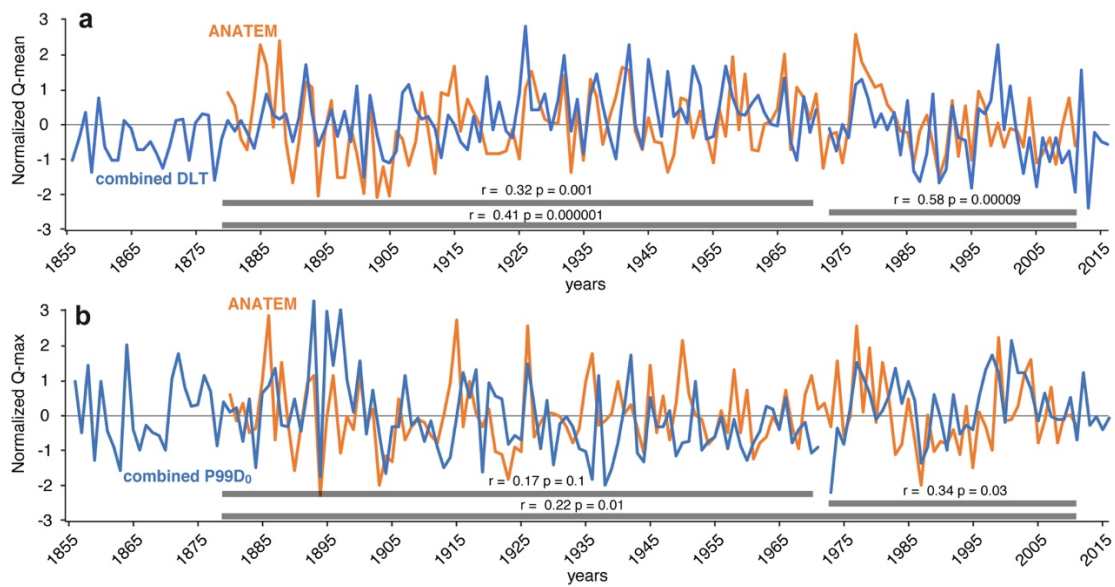
567 **4.7 Hydrological reconstruction using the rainfall-runoff modelling approach and**
568 **comparison with the varved-based reconstruction**

569 Naskaupi River Q-mean and Q-max (Fig. 8) were also reconstructed using the ANATEM
570 rainfall-runoff modelling (Fig. 10). The independent modelling approach results show
571 similarities with reconstructions based on varved series. The ANATEM reconstructions are
572 statistically and positively correlated with the yearly time series obtained from combined
573 DLT and P99D₀ series during the 1880-2011 period (Q-mean: $r = 0.41$; Q-max: $r = 0.22$; $n = 131$;
574 $p < 0.01$). The reconstructed Q-mean and Q-max annual variabilities show
575 similarities, especially during the 1973–2011 period (Q-mean: $r = 0.58$; Q-max: $r = 0.34$;
576 $n = 43$ $p < 0.05$).

577

578 Q-mean reconstructions with both varve parameters and modelling are better correlated
579 than the Q-max reconstructions. This may be due to the higher uncertainty related to the
580 Q-max reconstruction with the modelling approach. Indeed, high flow modelling requires
581 good reconstruction performances on several hydro-climatic processes (i.e., snow
582 accumulation during the winter, timing of the snowmelt, spring precipitation). Moreover,
583 the uncertainty of the hydrological reconstruction is less important on recent periods
584 (>1950), due to the better quality of the geopotential height field reanalysis over recent
585 decades, as more stations series are available and thus used in the reanalysis. The decrease

586 in the uncertainty related to reanalysis over time might explain the better correlation
587 between the two approaches for the recent period.



588

589 *Figure 10. Comparison between the Naskaupi River (a) Q-mean and (b) Q-max reconstruction using*
590 *combined Detrital Layer Thickness (DLT) (without the NAS-1 1972-2016 period) and P99D₀ series*
591 *respectively (blue line) and the rainfall-runoff modelling (orange line) for raw yearly data.*

592 **5. Discussion**

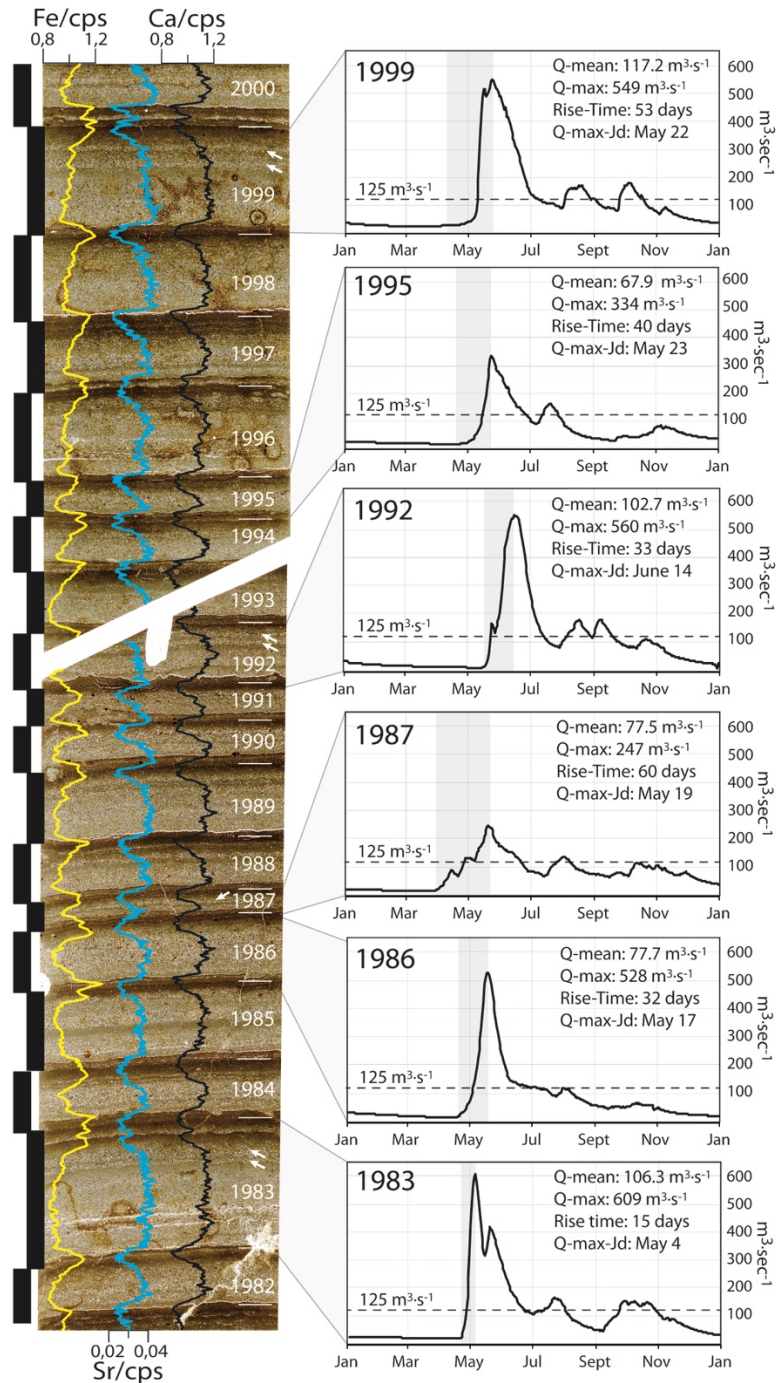
593 **5.1 Grand Lake varve formation**

594 Lakes containing well-defined and continuous varved sequences that allow the
595 establishment of an internal chronology are rare in boreal regions. However, the great depth
596 of Grand Lake, the availability of fine sediments in its watershed due to the glacial and
597 postglacial history of the region (Trottier et al., 2020), as well as its important seasonal
598 river inflow have favoured the formation and preservation of exquisite and thick varves.
599 The seasonal streamflow regime plays a significant role in the annual cycle of
600 sedimentation in Grand Lake and is responsible for the formation of the three distinct varve
601 layers. Due to the thickness and the clarity of the varve structures, it is possible to infer the
602 deposition mechanism for each layer and the season in which they were deposited.

603

604 The early spring layers are interpreted to be deposited during the river and lake ice break-
605 up and disintegration period, when erosion and resuspension of fine-grained sediments are
606 initiated but still low. Available Landsat-8 images of Grand Lake covering the 1983-2018
607 period (courtesy of the U.S. Geological Survey) shows that Grand Lake ice cover starts to
608 melt at the Naskaupi and Beaver River mouths. This ice melting pattern creates open bays
609 where drifting floating ice melts, thus depositing ice-rafted debris (Lamoureux 1999, 2004)
610 as observed in the early spring layer facies. The overlying detrital layers are interpreted as
611 flood-induced turbidites deposited at the lake bottom during the open-water season. High
612 energy sediment-laden river flows produce hyperpycnal flows allowing silt and sand-size
613 sediments to reach the cored sites (Cockburn and Lamoureux, 2008). The sharp contact
614 boundary between the early spring layer and the detrital layer at the top part of the early
615 spring layer supports the hypothesis that the detrital layers originate from underflows
616 (Mangili et al., 2005). The sediment waves on the Naskaupi and Beaver river delta slopes
617 (Trottier et al., 2020) (Fig. 1b, c) also indicate significant downstream sediment transport
618 by supercritical density flows (Normandeau et al., 2016). The thick and grading upward
619 basal part of the detrital layers are deposited during the high spring discharge period
620 generated by snowmelt runoffs. The lack of erosion marks between the early spring layer
621 and the detrital layer and the incorporation of rare cohesive sediment clasts within the
622 detrital layer suggests that erosion of the underlying early spring layers occurs in more

623 proximal and energetic settings. Three observations justify the combination of varve
624 measurements from the 3 coring sites : 1) the sedimentary processes inferred from the
625 observation of thin-sections, the high resolution bathymetric and the sub-bottom surveys
626 are similar; (2) the similarity of the varve facies and properties for each single year at the
627 3 different sites suggest a sedimentary pattern devoid of disturbances due to local factors;
628 (3) Grains-size differences are too subtle to infer different sedimentary processes and
629 environments. The upper part of varve structure in core NAS-1 show the most perceptible
630 different after 1972 (see discussion below). In spring, river discharge reaches its annual
631 peaks and sediment transport capacities that are then no longer reached during the rest of
632 the summer and autumn (Fig. 2, 3c, 11). However, the presence of thin coarser intercalated
633 sub-layers in the upper part of the detrital layer indicates that some rainfall events, as
634 observed in Fig. 11 (i.e., 1983, 1987, 1992, 1999) also contribute to deposition of sediments
635 in this layer. The overlying autumn and winter layer resulted from the settling and
636 flocculation of fine particles in non-turbulent condition from fall through the onset of lake
637 ice, forming a typical clay cap.



638

639 *Figure 11. Qualitative comparison between NAS-1A varves from thin-sections (delimited by the black bars)*
 640 *with the hydrographs of the Naskaupi River. Observed annual Q-mean and Q-max as well as the timing and*
 641 *rise time of the peak spring discharge are shown. Black dotted lines represent the discharge threshold of*
 642 *~125 m³·sec⁻¹. (1999, 1992, 1986, 1983) Strong spring floods associated with thick coarse varves. (1995,*
 643 *1987) Low spring floods associated with thin varves. (1999, 1992, 1987, 1983) Coarser intercalated sub-*
 644 *layers in the upper part of the detrital layer linked with summer and autumn high-discharge events. (1986)*
 645 *Strong spring flood with a low summer and autumn flow associated to a varve without substructure. Thin-*
 646 *sections are overlain by iron (Fe: yellow line), strontium (Sr: blue line), and calcium (Ca: black line) relative*
 647 *intensities. See Fig. 5 for thin-sections locations.*

648 **5.2 Anthropogenic influences on recent sedimentation**

649 Anthropogenic environmental impacts on watersheds can be preserved in varved lake
650 sediments (Zolitschka et al., 2015; Saarni et al., 2016; Czymzik et al., 2018). Changes
651 observed in physical parameters of the varves deposited pre- and post-1971 at the NAS
652 sites suggest that the effect of the dyke system on the Naskaupi River sediment inputs is
653 perceptible in the Grand Lake varved sequence. The well-developed layers of varves
654 deposited prior to 1972 from sites NAS-1 (Fig. 6b) and NAS-2, and the similarity between
655 TVT and DLT values and variations among all sites over the 1856-1971 period (Fig. 6d)
656 indicate that before the Naskaupi River diversion, seasonal sedimentation cycles appeared
657 to have reached a relative state of equilibrium. The reduction of nearly half of the area of
658 the Naskaupi River watershed due to its diversion in April 1971, reduced the water inflows
659 and changed the base level of the downstream river system. The rapid base level fall must
660 have triggered modifications of the fluvial dynamics from late-spring to winter 1971 (i.e.,
661 channel incision, bank destabilization, and upstream knickpoint migration), likely
662 increasing the availability of sediments in the river system. The Naskaupi River
663 spring/summer/autumn flood(s) of 1972 have then remobilized and transported a large
664 amount of newly available floodplain sediments. This major sediment discharge plunged
665 in Grand Lake and extended as hyperpycnal flow in the axis of the Naskapi River
666 depositing a thick and coarse-grained turbidite following the lake bathymetry. This 1972
667 marker bed suggests that the Naskaupi River diversion had an impact on sedimentation at
668 sites NAS-1 and NAS-2.

669
670 The increase in thickness and particle size values of varves deposited post-1971 in core
671 NAS-1 (Fig. 5a, 6d/e, 7b, 11) suggest that the diversion has affected sedimentation at this
672 site over time. During the 1972-2016 period, the river floodplain morphology must have
673 been in a re-equilibration phase favourable to erosion, sediment transport, and deposition
674 of coarser varves on the Naskaupi River delta slope. Since the river diversion,
675 sedimentation at NAS-1 site appears to have become more sensitive to maximum
676 discharges variations in spring than mean annual discharges. The sensitivity of the more
677 proximal NAS-1 site to Naskaupi River extreme discharges variability may partly explain
678 why better results are obtained without the 1972-2016 period to reconstruct Q-mean and

679 by keeping this period to the Q-max reconstruction. The negative correlation between
680 P99D₀ of the core NAS-1 and the timing and rise time of spring discharge (Table 3) also
681 demonstrate reactivity to spring entrainment energy conditions at this site. The distal NAS-
682 2 site shows that post-1971, sedimentation seems to have slightly lost sensitivity to river
683 discharge, and that sediment input continued to decline at the beginning of the deep lake
684 basin. The thin early spring layers free of ice-rafted debris in varve post-1971 of core NAS-
685 1 (Fig. 5a, 11) and NAS-2 indicate that the capacity of early spring discharge to transport
686 fine sediments and its ability to float ice to Grand Lake decreases along with the decrease
687 in water supplies.

688

689 It is tempting to link the decrease of varve thickness in core NAS-2 over the 1972- 2016
690 period with the discharge reduction due to the river diversion. However, similarities with
691 core BEA-1, a site devoid of anthropogenic perturbations (unaffected by the Naskaupi
692 River diversion) which also shows a decline in varve thickness, suggest that this decrease
693 can potentially be due to natural hydro-climatic conditions. The observed Naskaupi River
694 Q-mean series also show a decrease on the 1978-2011 period. Indeed, because of the distant
695 location of site BEA-1 from the Naskaupi River mouth, the diversion is most likely not
696 responsible for the decrease of varve thickness in this sector. Moreover, it is quite unlikely
697 that the sedimentary input from the Naskaupi River contributed to sediment accumulation
698 at the mouth of the Beaver River. The absence of any traces of the 1972 marker bed at the
699 Beaver River mouth (BEA-1) supports this hypothesis. Furthermore, the thickness decrease
700 observed in BEA-1 began after ~1920 (Fig. 6a), which is before the 1971 diversion.

701

702 Anthropogenic modification of the Naskaupi River watershed makes it challenging to
703 discuss natural hydroclimate-related variations before and after 1971. Some caution should
704 be applied when comparing pre- to post 1972 reconstructions, given the changes in
705 watershed conditions that happened after the construction of the system of dykes. There is
706 no instrumental data available for the Naskaupi River watershed before 1971 to confirm
707 that the calibration model post-diversion (1978-2011) is similarly robust for the preceding
708 period. The river diversion affected the Naskaupi River sedimentation dynamics but did
709 not modify it drastically. Despite the observed post-diversion changes in varves' physical

710 parameters in cores NAS-1 and NAS-2, which are however moderate, the varves still
711 responded directly to variations in river discharge. In addition, the part of the watershed
712 that has been diverted is an area composed mainly of lakes, which are not very
713 hydrologically reactive.

714 **5.3 The hydro-climatic signal in the varve record**

715 The significant correlations between continuous varve thickness and particle size
716 measurements with instrumental hydrological variables (Tab. 3) show that Grand Lake
717 varved sediments are reliable proxies to reconstruct past hydrologic conditions through
718 time at the annual to seasonal scale. The thick and/or coarse-grained varves correspond
719 well to years of high river discharges, whereas thin and/or fine-grained varves are related
720 with years of low discharge. Moreover, figure 11 clearly demonstrates how Grand Lake
721 varve record can be exploited to examine the interaction between meteorological
722 conditions and rivers discharge at an inter-seasonal scale, which is a temporal resolution
723 rarely obtained with natural proxies.

724

725 Data from the 3 sites were combined in order to better capture the regional hydroclimatic
726 signal and to somehow attenuate the noise that is inherent from the analysis of a single core
727 in a very large lake. A single core will be more sensitive to local specificities and is
728 probably less representative of the entire hydrogram. The Beaver and the Naskaupi Rivers
729 have adjacent catchments that share the same climatological and geological characteristics,
730 while the Beaver River's catchment is devoid of anthropogenic modifications. The
731 combination of varve parameters from different coring sites with distinct sediment sources
732 (Fig. 1b) improved the correlations with local and regional hydrological variables (Tab. 3)
733 and thereby the reconstructions (Fig. 8, 9). By integrating the core BEA into the combined
734 data, it allows to capture the hydrological signal from a larger region (Naskaupi + Beaver
735 watersheds) and it helps to capture the natural hydrological signal in our combined series
736 used for reconstructions.

737

738 As demonstrated by previous studies on varved sediments, the use of both varve thickness
739 and particle size analysis allows for a more specific investigation of the range of

740 hydroclimate conditions recorded within varves (Francus et al., 2002; Cockburn and
741 Lamoureux, 2008; Lapointe et al., 2012). For Grand Lake, the combined DLT is found to
742 be the best proxy to reconstruct all hydrological events occurring throughout the year (Q-
743 mean). DLT series are better at predicting Q-mean because the early spring layers and
744 autumn and winter layers thickness are more variable and are included in the TVT
745 measurements. This variability can be linked to specific climatic and geomorphological
746 parameters such as the duration of ice cover on Grand Lake and the Naskaupi River ice
747 breakup processes which induce noise in the hydrologic signal contained in TVT series.
748 The combined P99D₀ yields the strongest correlation in our dataset (Tab. 3) and is the best
749 proxy to reconstruct maximum annual discharges (Q-max). This result is logical because
750 the peak discharge is controlling the competence of the river and consequently the size of
751 the particles that can be transported. Moreover, this indicator is not sensitive to sediment
752 compaction, which may affect other proxies based on thickness.

753

754 The significant positive correlations between varve physical parameters and Snow-Win,
755 Q-nival (Tab. 3) and even Temp-Spring demonstrate that Grand Lake varve predominantly
756 reflects spring discharge conditions (e.g., Ojala and Alenius 2005; Lamoureux et al., 2006;
757 Saarni et al., 2016; Czymzik et al., 2018), which is the major component of the regional
758 streamflow regimes classified as nival (snowmelt-dominated) (Bonsal et al., 2019). In
759 boreal regions, the intensity and length of spring floods are controlled by the snow
760 accumulation during winter and by the temperature of the melting period (Hardy et al.,
761 1996; Snowball et al., 1999; Cockburn and Lamoureux, 2008; Ojala et al., 2013; Saarni et
762 al., 2017). The negative correlation between P99D₀ of the NAS-1 and the timing and rise
763 time of spring discharge suggests that early spring flows that increase rapidly are conducive
764 conditions for high entrainment energy and the deposition of coarser laminations on the
765 distal part of the delta slope (Fig. 11; site NAS-1). The erosion of detrital materials in early
766 spring increases when the snowmelt runoffs occur on soils that are not yet stabilized and
767 protected by vegetation (Ojala and Alenius 2005, Czymzik et al., 2018).

768

769 Intercalated sub-layers in the upper part of the detrital layer are interpreted to be produced
770 by summer or fall rainfall events (Fig. 11). Yet, the significant positive correlations

771 between varve thickness and Nb-days-SupQ80 suggests that a daily discharge of $\sim 125 \text{ m}^3 \cdot \text{s}^{-1}$
772 ¹ represents an approximate threshold above which the deposition of coarse sediments in
773 Grand Lake (detrital layers) is more likely to occur (Fig. 11) (e.g., Czymzik et al., 2010,
774 Kämpf et al., 2014). According to the instrumental data (Fig. 2, 11), such a discharge can
775 be generated during the summer/autumn period, confirming that rainfall events can indeed
776 be triggering the deposition of thin intercalated sub-layers observed in the upper part of the
777 detrital layers (Fig. 11). However, there is non-significant low correlations between varves
778 thickness and Ptot-Annual/Ptot-Sum (not shown) suggesting that rainfalls contributions to
779 TVT remain small. These rainfall events have no contribution to P99D₀ because the
780 coarsest particles are found at the base of the detrital layers.

781

782 The comparison between the Naskaupi River hydro-climatic variables and other Labrador
783 hydrometric stations (Fig. 3) show that a coherent regional hydrological pattern exists in
784 the Labrador region. The performed regional Q-mean reconstitution and validation (Fig. 9)
785 indicated that the Labrador region hydrologic signal is recorded in the Grand Lake varve
786 sequence. The local and regional Q-mean reconstructed from the combined DLT series
787 (without the NAS-1 1972-2016 period) suggest a statistically significant decreasing trend
788 in mean annual discharge during the last 90 years. Naskaupi River Q-mean and Q-max
789 reconstructions based on both varve series and rainfall-runoff modelling revealed high
790 value periods from 1975 to 1985 and 1995 to 2005, and low values from 1986 to 1994 and
791 2006 to 2016 (Fig. 10). These results agree with the downward trend of the annual
792 streamflow observed in eastern Canada during the 20th century in other studies and also
793 with the reported higher river discharges from 1970 to 1979 and 1990 to 2007, and lower
794 discharges from 1980 to 1989 (Zhang et al. 2001; Sveinsson et al., 2008; Jandhyala et al.,
795 2009; Déry et al., 2009; Mortsch et al., 2015; Dinis et al., 2019).

796

797 In addition to providing a new high-quality varved record in eastern Canada, this research
798 highlights the complementarity between palaeohydrological reconstructions extracted
799 from clastic varved sediments and rainfall-runoff modelling. Both methods independently
800 offer a similar, yet robust, centennial perspective on river discharge variability in an
801 important region for the economic and sustainable development of water resources in

802 Canada. Reconstructed long-term mean and maximum annual river discharges series
803 provide valuable quantitative information particularly for water supply management for
804 hydropower generation and the estimation of flood and drought hazards. The varved
805 sediment of Grand Lake also allows documenting the effect of dyke systems on the
806 downstream sediment transport dynamic into a watershed and its implication for
807 palaeohydrological reconstruction. Further investigation of the impacts of the Naskaupi
808 watershed reduction on sediment transport could help better refine these reconstructions.
809 Future work in Grand Lake should be directed towards the high-resolution analysis of long
810 sediment cores in order to produce longer reconstructions. The Grand Lake deeper varved
811 sequence potentially recorded the hydro-climatic variability that occurred during the Late
812 Holocene in region sensitive to the North Atlantic climate, allowing interesting prospects
813 into large-scale atmospheric and oceanic modes of variability.

814

815 **6. Conclusions**

816 The great depth of Grand Lake, the availability of fine sediments along its tributaries, and
817 its important seasonal river inflow have favoured the formation and preservation of fluvial
818 clastic laminated sediments. By using a new varved record in eastern Canada and a rainfall-
819 runoff modelling approach, this paper provides a better understanding of the recording of
820 hydro-climatic conditions in large and deep boreal lakes and allows extending the
821 hydrological series beyond the instrumental period as well as the spatial coverage of the
822 rare annual palaeohydrological proxies in North America. The key results of this study are:

- 823 • The annual character of the 160 years-long lamination sequence has been confirmed.
824 Each varve, composed of an early spring layer, a summer/autumn detrital layer and an
825 autumn and winter layer, represents one hydrological year.
- 826 • Grand Lake varve formation is mainly related to the largest hydrological event of the
827 year, the spring discharge, with minor contributions from summer and autumn rainfall
828 events.
- 829 • Two hydrological parameters, the Naskaupi river Q-mean and Q-max annual
830 discharges, are robustly reconstructed from two independent varves physical
831 parameters, i.e., the detrital layer thickness (DLT) and grain size (P99D₀) respectively,
832 over the 1856-2016 period. The reconstructed Q-mean series suggest that high Q-mean

833 years occurred during the 1920-1960 period and a decrease in Q-mean takes place
834 during the second half of the 20th century.

835 • The same two hydrological parameters (Q-mean and Q-max), were also reconstructed
836 using the ANATEM rainfall-runoff modelling. ANATEM discharges series show
837 similarities with reconstructions based on the varved series, which support the
838 reliability of the two independent reconstruction approaches.

839 • The statistically significant relation between combined DLT series and the observed
840 Labrador region Q-mean series, extracted from five watersheds of different size and
841 location, demonstrates that Grand Lake varved sequence can also be used as a proxy of
842 regional river discharges conditions.

843 • The effects of Naskaupi River dyking in 1971 are clearly visible in the sedimentary
844 record and affected sedimentary patterns afterwards. While this event makes the
845 hydroclimatic reconstruction trickier, it remains that the outstanding quality of this
846 varved sequence provides one of the best hydroclimatic reconstruction from a
847 sedimentary record, with Pearson correlation coefficients up to $r = 0.75$.

848

849 **Data availability**

850 The data set used in this study will be available on the PANGAEA database.

851

852 **Author contributions**

853 This study is part of AGP's thesis under the supervision of PF and PL. AT and PL provided
854 geophysical data (Fig. 1b, c) and useful information on the morpho-stratigraphical
855 framework of Grand Lake. AGP and DF conducted the coring fieldtrip. AGP and PB
856 collected instrumental data. PB calculated hydro-climatic variables from instrumental data
857 (Fig. 3) and performed the rainfall-runoff modelling. HD and AGP adapted the code used
858 to establish the relationship between the varve parameters and the instrumental data and
859 for the regression model. AGP performed most of the data analysis, wrote the manuscript
860 and created the figures with contributions from PF and PB. All authors provided valuable
861 feedback and contributed to the improvement of the manuscript.

862

863 **Competing interests**

864 The author Pierre Francus is a member of the editorial board of the journal.

865

866 **Acknowledgments**

867 This research was financially supported by NSERC-Ouranos-Hydro-Québec-Hydro-
868 Manitoba through a CRD grant to P.F. and P.L. (PERSISTANCE project, É. Boucher et
869 al.). This work was also supported by the FRQNT through a doctoral (B2X) research
870 scholarship to A.G.P. and by the MOPGA Short Stay program grant at Université Côte
871 d'Azur, Nice, France to A.G.P and P.B. A financial support for the fieldwork campaign at
872 Grand Lake was provided by POLAR through the NSTP program to A.G.P. The authors
873 are grateful to Arnaud De Coninck, David Deligny and Louis-Frédéric Daigle for their
874 participation during fieldwork, laboratory and helpful discussions. We greatly thank
875 Wanda and Dave Blake from North West River for their guiding experience and
876 accommodation at Grand Lake. We thank the Labrador Institute at North West River for
877 the use of their facility during fieldwork. We want to thank Stéphane Ferré from the Micro-
878 Geoarchaeology Laboratory of the Center for Northern Studies (CEN) in Québec, QC,
879 Canada, for the production of the high-quality thin-sections used in this study. We would

880 also like to thank the three reviewers for their constructive review of this article. Finally,
881 many thanks to Monique Gagnon, Charles Smith and Clarence Gagnon for reviewing the
882 English of an earlier version of the manuscript.

883 **References**

884 Amann, B., Szidat, S., and Grosjean, M.: A millennial-long record of warm season
885 precipitation and flood frequency for the North-western Alps inferred from varved lake
886 sediments: implications for the future, *Quaternary. Sci. Rev.*, 115, 89-100,
887 <https://doi.org/10.1016/j.quascirev.2015.03.002>, 2015.

888
889 Anderson, T.: *Rivers of Labrador*, Canadian Special Publication of Fisheries and Aquatic
890 Sciences 81, Ottawa, Ontario, 1985.

891
892 Appleby, P. and Oldfield, F.: The calculation of lead-210 dates assuming a constant rate of
893 supply of unsupported 210Pb to the sediment, *Catena*, 5, 1-8,
894 [https://doi.org/10.1016/S0341-8162\(78\)80002-2](https://doi.org/10.1016/S0341-8162(78)80002-2), 1978.

895
896 Bégin, C., Gingras, M., Savard, M. M., Marion, J., Nicault, A., and Bégin, Y.: Assessing
897 tree-ring carbon and oxygen stable isotopes for climate reconstruction in the Canadian
898 northeastern boreal forest, *Palaeogeography, Palaeoclimatology, Palaeoecology*, 423, 91-
899 101, <https://doi.org/10.1016/j.palaeo.2015.01.021>, 2015.

900
901 Bégin, Y., Nicault, A., Bégin, C., Savard, M. M., Arseneault, D., Berninger, F., Guiot, J.,
902 Boreux, J.-J., and Perreault, L.: Analyse dendrochronologique des variations passées du
903 régime hydro climatique au complexe de la grande rivière dans le Nord du Québec, *La*
904 *Houille Blanche*, 2007. 70-77, <https://doi.org/10.1051/lhb:2007085>, 2007.

905
906 Bonsal, B.R., Peters, D.L., Seglenieks, F., Rivera, A., and Berg, A.: Changes in freshwater
907 availability across Canada; Chapter 6 in *Canada's Changing Climate Report*, (ed.) E. Bush
908 and D.S. Lemmen; Government of Canada, Ottawa, Ontario, 2019.

909
910 Boucher, E., Nicault, A., Arseneault, D., Bégin, Y., and Karami, M. P.: Decadal Variations
911 in Eastern Canada's Taiga Wood Biomass Production Forced by Ocean-Atmosphere
912 Interactions, *Sci. Rep. Uk.*, 7, 1-13, <https://doi.org/10.1038/s41598-017-02580-9>, 2017.

913
914 Boucher, É., Ouarda, T. B., Bégin, Y., and Nicault, A.: Spring flood reconstruction from
915 continuous and discrete tree ring series, *Water. Resour. Res.*, 47,
916 <https://doi.org/10.1029/2010WR010131>, 2011.

917
918 Briffa, K., Jones, P., Pilcher, J., and Hughes, M.: Reconstructing summer temperatures in
919 northern Fennoscandia back to AD 1700 using tree-ring data from Scots pine, *Arct.*
920 *Antartic. Alp. Research.*, 20, 385-394, <https://doi.org/10.1080/00040851.1988.12002691>,
921 1988.

922

923 Brigode, P., Brissette, F., Nicault, A., Perreault, L., Kuentz, A., Mathevet, T., and Gailhard,
924 J.: Streamflow variability over the 1881–2011 period in northern Québec: comparison of
925 hydrological reconstructions based on tree rings and geopotential height field reanalysis,
926 *Clim. Past*, 12, 1785-1804, <https://doi.org/10.5194/cp-12-1785-2016>, 2016.

927

928 Cherry, J. E., Knapp, C., Trainor, S., Ray, A. J., Tedesche, M., and Walker, S.: Planning
929 for climate change impacts on hydropower in the Far North, *Hydrol. Earth Syst. Sci.*, 21,
930 133, <https://doi.org/10.5194/hess-21-133-2017>, 2017.

931

932 Cockburn, J. M. and Lamoureux, S. F.: Inflow and lake controls on short-term mass
933 accumulation and sedimentary particle size in a High Arctic lake: implications for
934 interpreting varved lacustrine sedimentary records, *J. Paleolimnol.*, 40, 923-942,
935 <https://doi.org/10.1007/s10933-008-9207-5>, 2008.

936

937 Collins, M., Knutti, R., Arblaster, J., Dufresne, J-L., Fichefet, T., Friedlingstein, P., Gao,
938 X., Gutowski, W. J., Johns, T., Krinner, G., Shongwe, M., Tebaldi, C., Weaver, A. J.,
939 Wehner, M. F., Allen, M. R., Andrews, T., Beyerle, U., Bitz, C. M., Bony, S., & Booth, B.
940 B. B.: Long-term climate change: projections, commitments and irreversibility, In: *Climate
941 Change 2013 - The Physical Science Basis, Contribution of Working Group I to the Fifth
942 Assessment Report of the Intergovernmental Panel on Climate Change, Intergovernmental
943 Panel on Climate Change, Cambridge University Press, 1029-1136, 2013.*

944

945 Compo, G. P., Whitaker, J. S., Sardeshmukh, P. D., Matsui, N., Allan, R. J., Yin, X.,
946 Gleason, B. E., Vose, R. S., Rutledge, G., and Bessemoulin, P.: The twentieth century
947 reanalysis project, *Q J R Meteorol Soc*, 137, 1-28, <https://doi.org/10.1002/qj.776>, 2011.

948

949 Cook, E. R., Meko, D. M., Stahle, D. W., and Cleaveland, M. K.: Drought reconstructions
950 for the continental United States, *J. Clim.*, 12, 1145-1162, [https://doi.org/10.1175/1520-
951 0442\(1999\)012%3C1145:DRFTCU%3E2.0.CO;2](https://doi.org/10.1175/1520-0442(1999)012%3C1145:DRFTCU%3E2.0.CO;2), 1999.

952

953 Coron, L., Thirel, G., Delaigue, O., Perrin, C., and Andréassian, V.: The suite of lumped
954 GR hydrological models in an R package, *Environmental Modelling & Software*, 94, 166-
955 171, <https://doi.org/10.1016/j.envsoft.2017.05.002>, 2017.

956

957 Croudace, I. W., Rindby, A., and Rothwell, R. G.: ITRAX: description and evaluation of a
958 new multi-function X-ray core scanner, *Geological Society, London, Special Publications*,
959 267, 51-63, <https://doi.org/10.1144/GSL.SP.2006.267.01.04>, 2006.

960

961 Coven, S., Francus, P., and Lamoureux, S.: Mid to Late Holocene hydroclimatic and
962 geochemical records from the varved sediments of East Lake, Cape Bounty, Canadian High

963 Arctic, Quaternary. Sci. Rev., 30, 2651-2665,
964 <https://doi.org/10.1016/j.quascirev.2011.05.019>, 2011.
965
966 Cuvén, S., Francus, P., and Lamoureux, S. F.: Estimation of grain size variability with
967 micro X-ray fluorescence in laminated lacustrine sediments, Cape Bounty, Canadian High
968 Arctic, *J. Paleolimnol.*, 44, 803-817, <https://doi.org/10.1007/s10933-010-9453-1>, 2010.
969
970 Czymzik, M., Dulski, P., Plessen, B., Von Grafenstein, U., Naumann, R., and Brauer, A.:
971 A 450 year record of spring-summer flood layers in annually laminated sediments from
972 Lake Ammersee (southern Germany), *Water. Resour. Res.*, 46,
973 <https://doi.org/10.1029/2009WR008360>, 2010.
974
975 Czymzik, M., Haltia, E., Saarni, S., Saarinen, T., and Brauer, A.: Differential North
976 Atlantic control of winter hydroclimate in late Holocene varved sediments of Lake
977 Kortejärvi, eastern Finland, *Boreas*, 47, 926-937, <https://doi.org/10.1111/bor.12315>, 2018.
978
979 D'Arrigo, R., Buckley, B., Kaplan, S., and Woollett, J.: Interannual to multidecadal modes
980 of Labrador climate variability inferred from tree rings, *Clim. Dynam.*, 20, 219-228,
981 <https://doi.org/10.1007/s00382-002-0275-3>, 2003.
982
983 Déry, S. J. and Wood, E. F.: Decreasing river discharge in northern Canada, *Geophys. Res.*
984 *Lett.*, 32, <https://doi.org/10.1029/2005GL022845>, 2005.
985
986 Dinis, L., Bégin, C., Savard, M. M., Marion, J., Brigode, P., and Alvarez, C.: Tree-ring
987 stable isotopes for regional discharge reconstruction in eastern Labrador and
988 teleconnection with the Arctic Oscillation, *Clim. Dynam.*, 53, 3625-3640,
989 <https://doi.org/10.1007/s00382-019-04731-2>, 2019.
990
991 Fitzhugh, W.: Environmental Approaches to the Prehistory of the North, *Journal of the*
992 *Washington Academy of Sciences*, 1973. 39-53, 1973.
993
994 Francus, P.: An image-analysis technique to measure grain-size variation in thin sections
995 of soft clastic sediments, *Sedimentary Geology*, 121, 289-298,
996 [https://doi.org/10.1016/S0037-0738\(98\)00078-5](https://doi.org/10.1016/S0037-0738(98)00078-5), 1998.
997
998 Francus, P., Bradley, R. S., Abbott, M. B., Patridge, W., and Keimig, F.: Paleoclimate
999 studies of minerogenic sediments using annually resolved textural parameters, *Geophys.*
1000 *Res. Lett.*, 29, 59-51-59-54, <https://doi.org/10.1029/2002GL015082>, 2002.
1001

1002 Francus, P. and Cosby, C. A.: Sub-sampling unconsolidated sediments: A solution for the
1003 preparation of undisturbed thin-sections from clay-rich sediments, *J. Paleolimnol*, 26, 323-
1004 326, <https://doi.org/10.1023/A:1017572602692>, 2001.
1005
1006 Francus, P. and Karabanov, E.: A computer-assisted thin-section study of Lake Baikal
1007 sediments: a tool for understanding sedimentary processes and deciphering their climatic
1008 signal, *Int. J. Earth. Sci.*, 89, 260-267, <https://doi.org/10.1007/s005319900064>, 2000.
1009
1010 Francus, P., Keimig, F., and Besonen, M.: An algorithm to aid varve counting and
1011 measurement from thin-sections, *Journal of Paleolimnology*, 28, 283-286,
1012 <https://doi.org/10.1023/A:1021624415920>, 2002.
1013
1014 Francus, P. and Nobert, P.: An integrated computer system to acquire, process, measure
1015 and store images of laminated sediments, In 4th International limnogeology congress,
1016 Barcelona, July, 2007.
1017
1018 Fulton, R. J. and Ferguson, J.: *Surficial Geology Cartwright: Labrador, Newfoundland,*
1019 *Commission, Department of Energy, Mines and Resources*, 1986.
1020
1021 Gilbert, R. and Desloges, J. R.: Late glacial and Holocene sedimentary environments of
1022 Quesnel Lake, British Columbia, *Geomorphology*, 179, 186-196,
1023 <https://doi.org/10.1016/j.geomorph.2012.08.010>, 2012.
1024
1025 Gupta, H. V., Kling, H., Yilmaz, K. K., and Martinez, G. F.: Decomposition of the mean
1026 squared error and NSE performance criteria: Implications for improving hydrological
1027 modelling, *J. Hydrol.*, 377, 80-91, <https://doi.org/10.1016/j.jhydrol.2009.08.003>, 2009.
1028
1029 Hardy, D. R., Bradley, R. S., and Zolitschka, B.: The climatic signal in varved sediments
1030 from Lake C2, northern Ellesmere Island, Canada, *J. Paleolimnol.*, 16, 227-238,
1031 <https://doi.org/10.1007/BF00176938>, 1996.
1032
1033 Heideman, M., Menounos, B., and Clague, J. J.: An 825-year long varve record from
1034 Lillooet Lake, British Columbia, and its potential as a flood proxy, *Quaternary. Sci. Rev.*,
1035 126, 158-174, <https://doi.org/10.1016/j.quascirev.2015.08.017>, 2015.
1036
1037 Jandhyala, V. K., Liu, P., and Fotopoulos, S. B.: River stream flows in the northern Québec
1038 Labrador region: A multivariate change point analysis via maximum likelihood, *Water.*
1039 *Resour. Res.*, 45, <https://doi.org/10.1029/2007WR006499>, 2009.
1040
1041 Kämpf, L., Brauer, A., Swierczynski, T., Czymzik, M., Mueller, P., and Dulski, P.:
1042 Processes of flood-triggered detrital layer deposition in the varved Lake Mondsee sediment

1043 record revealed by a dual calibration approach, *Journal of Quaternary Science*, 29, 475-
1044 486, <https://doi.org/10.1002/jqs.2721>, 2014.

1045

1046 Kaufman, C. A., Lamoureux, S. F., and Kaufman, D. S.: Long-term river discharge and
1047 multidecadal climate variability inferred from varved sediments, southwest Alaska, *Quat.*
1048 *Res.*, 76, 1-9, <https://doi.org/10.1016/j.yqres.2011.04.005>, 2011.

1049

1050 Kuentz, A., Mathevet, T., Gailhard, J., and Hingray, B.: Building long-term and high
1051 spatio-temporal resolution precipitation and air temperature reanalyses by mixing local
1052 observations and global atmospheric reanalyses: the ANATEM model, *Hydrol. Earth Syst.*
1053 *Sci.*, 19, 2717-2736, <https://doi.org/10.5194/hess-19-2717-2015>, 2015.

1054

1055 Kylander, M. E., Ampel, L., Wohlfarth, B., and Veres, D.: High-resolution X-ray
1056 fluorescence core scanning analysis of Les Echets (France) sedimentary sequence: new
1057 insights from chemical proxies, *J. Quat. Sci.*, 26, 109-117,
1058 <https://doi.org/10.1002/jqs.1438>, 2011.

1059

1060 Lamoureux, S.: Five centuries of interannual sediment yield and rainfall-induced erosion
1061 in the Canadian High Arctic recorded in lacustrine varves, *Water. Resour. Res.*, 36, 309-
1062 318, <https://doi.org/10.1029/1999WR900271>, 2000.

1063

1064 Lamoureux, S. F.: Embedding unfrozen lake sediments for thin section preparation, *J.*
1065 *Paleolimnol.*, 10, 141-146, <https://doi.org/10.1007/BF00682510>, 1994.

1066

1067 Lamoureux, S. F., Stewart, K. A., Forbes, A. C., and Fortin, D.: Multidecadal variations
1068 and decline in spring discharge in the Canadian middle Arctic since 1550 AD, *Geophys.*
1069 *Res. Lett.*, 33, <https://doi.org/10.1029/2005GL024942>, 2006.

1070

1071 Lapointe, F., Francus, P., Lamoureux, S. F., Saïd, M., and Cuvén, S.: 1750 years of large
1072 rainfall events inferred from particle size at East Lake, Cape Bounty, Melville Island,
1073 Canada, *J. paleolimnol.*, 48, 159-173, <https://doi.org/10.1007/s10933-012-9611-8>, 2012.

1074

1075 Linderholm, H. W., Nicolle, M., Francus, P., Gajewski, K., Helama, S., Korhola, A.,
1076 Solomina, O., Yu, Z., Zhang, P., D'Andrea, W. J., Debret, M., Divine, D. V., Gunnarson,
1077 B. E., Loader, N. J., Massei, N., Seftigen, K., Thomas, E. K., Werner, J., Andersson, S.,
1078 Berntsson, A., Luoto, T. P., Nevalainen, L., Saarni, S., and Väiliranta, M.: Arctic
1079 hydroclimate variability during the last 2000 years: current understanding and research
1080 challenges, *Clim. Past*, 14, 473–514, <https://doi.org/10.5194/cp-14-473-2018>, 2018.

1081

1082 Ljungqvist, F. C., Krusic, P. J., Sundqvist, H. S., Zorita, E., Brattström, G., and Frank, D.:
1083 Northern Hemisphere hydroclimate variability over the past twelve centuries, *Nature*, 532,
1084 94-98, <https://doi.org/10.1038/nature17418>, 2016.

1085

1086 Mangili, C., Brauer, A., Moscardiello, A., and Naumann, R.: Microfacies of detrital event
1087 layers deposited in Quaternary varved lake sediments of the Piànico-Sèllere Basin
1088 (northern Italy), *Sedimentology*, 52, 927-943, [https://doi.org/10.1111/j.1365-](https://doi.org/10.1111/j.1365-3091.2005.00717.x)
1089 [3091.2005.00717.x](https://doi.org/10.1111/j.1365-3091.2005.00717.x), 2005.

1090

1091 Mortsch, L., Cohen, S., and Koshida, G.: Climate and water availability indicators in
1092 Canada: Challenges and a way forward. Part II–Historic trends, *Can. Water Resour. J.*, 40,
1093 146-159, <https://doi.org/10.1080/07011784.2015.1006024>, 2015.

1094

1095 Naulier, M., Savard, M. M., Bégin, C., Gennaretti, F., Marion, J., Nicault, A., and Bégin,
1096 Y.: A millennial summer temperature reconstruction for northeastern Canada using oxygen
1097 isotopes in subfossil trees, *Clim. Past*, 11, 1153-1164, [https://doi.org/10.5194/cp-11-1153-](https://doi.org/10.5194/cp-11-1153-2015)
1098 [2015](https://doi.org/10.5194/cp-11-1153-2015), 2015.

1099

1100 Nicault, A., Boucher, E., Bégin, C., Guiot, J., Marion, J., Perreault, L., Roy, R., Savard, M.
1101 M., and Bégin, Y.: Hydrological reconstruction from tree-ring multi-proxies over the last
1102 two centuries at the Caniapiscou Reservoir, northern Québec, Canada, *J. Hydrol.*, 513, 435-
1103 445, <https://doi.org/10.1016/j.jhydrol.2014.03.054>, 2014.

1104

1105 Normandeau, A., Lajeunesse, P., Poiré, A. G., and Francus, P.: Morphological expression
1106 of bedforms formed by supercritical sediment density flows on four fjord-lake deltas of the
1107 south-eastern Canadian Shield (Eastern Canada), *Sedimentology*, 63, 2106-2129,
1108 <https://doi.org/10.1111/sed.12298>, 2016.

1109

1110 Notzl, L., Greene, R., and Riley, J.: Labrador Nature Atlas. Vol. II. Ecozones, Ecoregions,
1111 and Ecodistricts, Nature Conservancy of Canada and Province of Newfoundland and
1112 Labrador, Toronto, ON, Canada, 2013.

1113

1114 Ojala, A. E. and Alenius, T.: 10 000 years of interannual sedimentation recorded in the
1115 Lake Nautajärvi (Finland) clastic–organic varves, *Palaeogeography, Palaeoclimatology,*
1116 *Palaeoecology*, 219, 285-302, <https://doi.org/10.1016/j.palaeo.2005.01.002>, 2005.

1117

1118 Ojala, A. E., Kosonen, E., Weckström, J., Korkkonen, S., and Korhola, A.: Seasonal
1119 formation of clastic-biogenic varves: the potential for palaeoenvironmental interpretations,
1120 *GFF*, 135, 237-247, <https://doi.org/10.1080/11035897.2013.801925>, 2013.

1121

1122 Oudin, L., Hervieu, F., Michel, C., Perrin, C., Andréassian, V., Anctil, F., and Loumagne,
1123 C.: Which potential evapotranspiration input for a lumped rainfall–runoff model?: Part 2—
1124 Towards a simple and efficient potential evapotranspiration model for rainfall–runoff
1125 modelling, *J. Hydrol.*, 303, 290-306, <https://doi.org/10.1016/j.jhydrol.2004.08.026>, 2005.
1126
1127 Perrin, C., Michel, C., and Andréassian, V.: Improvement of a parsimonious model for
1128 streamflow simulation, *J. Hydrol.*, 279, 275-289, [https://doi.org/10.1016/S0022-](https://doi.org/10.1016/S0022-1694(03)00225-7)
1129 [1694\(03\)00225-7](https://doi.org/10.1016/S0022-1694(03)00225-7), 2003.
1130
1131 Rohde, R., Muller, R., Jacobsen, R., Muller, E., Perlmutter, S., Rosenfeld, A., Wurtele, J.,
1132 Groom, D., and Wickham, C.: A New Estimate of the Average Earth Surface Land
1133 Temperature Spanning 1753 to 2011, *Geoinfor. Geostat.: An Overview 1: 1, of, 7, 2,*
1134 <http://dx.doi.org/10.4172/2327-4581.1000101>, 2013.
1135
1136 Saarni, S., Lensu, A., Tammelin, M., Haltia, E., and Saarinen, T.: Winter climate signal in
1137 boreal clastic-biogenic varves: a comprehensive analysis of three varved records from 1890
1138 to 1990 AD with meteorological and hydrological data from Eastern Finland, *GFF*, 139,
1139 314-326, <https://doi.org/10.1080/11035897.2017.1389984>, 2017.
1140
1141 Saarni, S., Saarinen, T., and Dulski, P.: Between the North Atlantic Oscillation and the
1142 Siberian High: A 4000-year snow accumulation history inferred from varved lake
1143 sediments in Finland, *Holocene*, 26, 423-431, <https://doi.org/10.1177/0959683615609747>,
1144 2016.
1145
1146 Schillereff, D. N., Chiverrell, R. C., Macdonald, N., and Hooke, J. M.: Flood stratigraphies
1147 in lake sediments: A review, *Earth-Sci. Rev.*, 135, 17-37,
1148 <https://doi.org/10.1016/j.earscirev.2014.03.011>, 2014.
1149
1150 Seiller, G., Anctil, F., and Perrin, C.: Multimodel evaluation of twenty lumped hydrological
1151 models under contrasted climate conditions, *Hydrol. Earth Syst. Sci.*,
1152 <https://dx.doi.org/10.5194/hess-1116-1171-2012>, 2012.
1153
1154 Snowball, I., Sandgren, P., and Petterson, G.: The mineral magnetic properties of an
1155 annually laminated Holocene lake-sediment sequence in northern Sweden, *Holocene*, 9,
1156 353-362, <https://doi.org/10.1191/095968399670520633>, 1999.
1157
1158 St-Onge, G., Mulder, T., Francus, P., and Long, B.: Chapter two continuous physical
1159 properties of cored marine sediments, *Developments in marine geology*, 1, 63-98,
1160 [https://doi.org/10.1016/S1572-5480\(07\)01007-X](https://doi.org/10.1016/S1572-5480(07)01007-X), 2007.
1161

1162 Stocker, T. F., Qin, D., Plattner, G.-K., Tignor, M. M., Allen, S. K., Boschung, J., Nauels,
1163 A., Xia, Y., Bex, V., and Midgley, P. M.: Climate change 2013: the physical science basis.
1164 Contribution of working group I to the fifth assessment report of IPCC the
1165 intergovernmental panel on climate change. Cambridge University Press,
1166 <https://dx.doi.org/10.1017/CBO9781107415324>, 2014.
1167

1168 Sturm, M.: Origin and composition of clastic varves, In: Schlüchter, C. (Ed.), Moraines
1169 and Varves: Origin, Genesis, Classification. A.A. Balkema, Rotterdam, The Netherlands,
1170 281-285, [https://www.worldcat.org/title/moraines-and-varves-origin-genesis-
1171 classification/oclc/5542145](https://www.worldcat.org/title/moraines-and-varves-origin-genesis-classification/oclc/5542145), 1979.
1172

1173 Sveinsson, O. G., Lall, U., Fortin, V., Perrault, L., Gaudet, J., Zebiak, S., and Kushnir, Y.:
1174 Forecasting spring reservoir inflows in Churchill Falls basin in Quebec, Canada, J. Hydrol.
1175 Eng., 13, 426-437, [https://dx.doi.org/10.1061/\(Asce\)1084-0699\(2008\)13:6\(426\)](https://dx.doi.org/10.1061/(Asce)1084-0699(2008)13:6(426)), 2008.
1176

1177 R Core Team: R: A Language and Environment for Statistical Computing, R Foundation
1178 for Statistical Computing, Vienna, Austria, <http://www.R-project.org/>, 2019.
1179

1180 Tomkins, J. D., Lamoureux, S. F., Antoniades, D., and Vincent, W. F.: Autumn snowfall
1181 and hydroclimatic variability during the past millennium inferred from the varved
1182 sediments of meromictic Lake A, northern Ellesmere Island, Canada, Quat. Res., 74, 188-
1183 198, <https://doi.org/10.1016/j.yqres.2010.06.005>, 2010.
1184

1185 Trottier, A. P., Lajeunesse, P., Gagnon-Poiré, A., and Francus, P.: Morphological
1186 signatures of deglaciation and postglacial sedimentary processes in a deep fjord-lake
1187 (Grand Lake, Labrador), Earth Surf. Proc. Land., 45, 928-947,
1188 <https://doi.org/10.1002/esp.4786>, 2020.
1189

1190 Valéry, A., Andréassian, V., and Perrin, C.: ‘As simple as possible but not simpler’: What
1191 is useful in a temperature-based snow-accounting routine? Part 1–Comparison of six snow
1192 accounting routines on 380 catchments, J. Hydrol, 517, 1166-1175,
1193 <https://doi.org/10.1016/j.jhydrol.2014.04.059>, 2014a.
1194

1195 Valéry, A., Andréassian, V., and Perrin, C.: ‘As simple as possible but not simpler’: What
1196 is useful in a temperature-based snow-accounting routine? Part 2–Sensitivity analysis of
1197 the Cemaneige snow accounting routine on 380 catchments, J. Hydrol., 517, 1176-1187,
1198 <https://doi.org/10.1016/j.jhydrol.2014.04.058>, 2014b.
1199

1200 Viau, A. E. and Gajewski, K.: Reconstructing millennial-scale, regional paleoclimates of
1201 boreal Canada during the Holocene, *J. Clim.*, 22, 316-330,
1202 <https://doi.org/10.1175/2008JCLI2342.1>, 2009.
1203
1204 Zang, C. and Biondi, F.: treeclim: an R package for the numerical calibration of proxy-
1205 climate relationships, *Ecography*, 38, 431-436, [10.1111/ecog.01335](https://doi.org/10.1111/ecog.01335), 2015.
1206
1207 Zhang, X., Harvey, K. D., Hogg, W., and Yuzyk, T. R.: Trends in Canadian streamflow,
1208 *Water Resour. Res.*, 37, 987-998, <https://doi.org/10.1029/2000WR900357>, 2001.
1209
1210 Zolitschka, B., Francus, P., Ojala, A. E., and Schimmelmann, A.: Varves in lake
1211 sediments—a review, *Quaternary. Sci. Rev.*, 117, 1-41,
1212 <https://doi.org/10.1016/j.quascirev.2015.03.019>, 2015.